UNIVERSITÀ DEGLI STUDI FIRENZE

DOTTORATO DI RICERCA TOSCANO IN NEUROSCIENZE

CICLO XXXII

COORDINATORE Prof. Renato Corradetti

Linked structural-functional brain abnormalities in patients with multiple sclerosis

Settore Scientifico Disciplinare MED/26

Dottorando

Dott. Zhang Jian

Jian Zhang

(firma)

Tutor

Prof. De Stefano Nicola

(firma)

Coordinatore

Prof. (*Cognome e Nome)*

(firma)

Anni 2016/2019

Table of Contents

1 Introduction

Multiple sclerosis (MS) is a widespread inflammatory, demyelinating and neurodegenerative disease of the central nervous system (CNS) (Filippi *et al.*, 2018*a*). Various lines of evidence from magnetic resonance image (MRI) have proven that MS results in multiple structural abnormalities, in terms of grey matter (GM) atrophy (Rocca *et al.*, 2017), white matter (WM) lesions and microstructural damage (Enzinger *et al.*, 2015, Filippi *et al.*, 2019*a*) as well as in functional connectivity abnormalities (Rocca *et al.*, 2015; Filippi *et al.*, 2017).

Recently, some studies suggested that WM damage may be spatially linked with subsequent cortical and deep GM atrophy in primary progressive and longstanding MS (Steenwijk *et al.*, 2014, 2016; Bodini *et al.*, 2016). Other studies showed that most of the cortical GM atrophy may be partially independent from the WM lesions in both early and progressive MS (Kawachi and Lassmann, 2017; Zurawski *et al.*, 2017). Few recent studies have revealed in MS, at the level of "patterns" (i.e., co-varying structurally and/or functionally related regions of the human brain), the presence of GM atrophy (Steenwijk *et al.*, 2016; Bergsland *et al.*, 2018) or WM microstructural damage (Meijer *et al.*, 2016), through source-based morphometry (SBM), a novel model-free and data-driven multivariate MRI-based approach, allowing grouping brain structural abnormalities into spatial patterns, well beyond the traditional assessment of single brain regions (Gupta *et al.*, 2015). We used here SBM on MRI data of a MS patient cohort with relatively mild disability in order to assess whether and to what extent distinct spatial patterns of GM atrophy and WM microstructural damage exist and may be inter-related.

Given the alterations found in both structural and functional MRI modalities in MS, integration across such modalities might provide a more comprehensive view of the pathogenic substrates, by revealing important "hidden" relationships that could not be detected from a single MRI modality (Calhoun and Sui, 2016). Despite the development of different MRI techniques has improved the evaluation of the relationship between structure and function in MS brain, there is still a need to bridge the gap in linking such structural/functional changes in order to better clarify the picture of the MS pathogenic mechanisms (Rocca *et al.*, 2015, Filippi *et al.*, 2018*b*).

Multimodal neuroimaging data-driven approach, by searching for common information across modalities, could identify co-occurring changes across various brain measures, and thus yield a more comprehensive picture of the multiple underlying pathogenic mechanisms of disease (Groves *et al.*, 2011; Francx *et al.*, 2016; Wolfers *et al.*, 2017, Llera *et al.*, 2019*a*). In this regard, we aimed to uncover in MS the hidden relationships between brain structural damage and functional alterations and the shared pathophysiology across different MRI modalities from a system-level perspective, through the multivariate analysis of multimodal brain MRI data. Our results reinforce previous findings on single MRI modalities and, furthermore, allow to investigate more efficiently the intimate pathogenic mechanism of WM and GM damage in terms of coexisting structural and functional changes, even at early disease stage.

1.1 Epidemiology

In Italy, the estimated annual incidence of MS ranges from 1.1 to 9.7 cases per 100,000 population (Battaglia and Bezzini, 2017) while the female-to-male ratios for incidence range from 1.19:1 to 3:1 (Kingwell *et al.*, 2013). The prevalence varies from 20 to 188 cases per 100,000 population

(Battaglia and Bezzini, 2017). Age-standardized prevalence estimates increased by 31.7% between 1990 and 2016 (Wallin *et al.*, 2019). In 2016, an estimated 72,352 people in Italy had MS (Wallin *et al.*, 2019). There were 398 deaths due to MS (95% uncertainty interval [UI]: 280 to 475) and 29,059 disability-adjusted life-years (DALYs) (95% UI: 22,643 to 35,453) due to MS in 2016. Worldwide, an estimated 2,221,188 people had MS, corresponding to a prevalence of 30.1 cases per 100,000 population (Wallin *et al.*, 2019), with age-standardized prevalence estimates increased by 10.4% between 1990 and 2016 (Wallin *et al.*, 2019). Among preteen children, the prevalence of MS is similar in boys and girls, in contrast to the end of the sixth decade of life, when the sex ratio is 2:1 in favor of women (Wallin *et al.*, 2019). There were 18,932 deaths due to MS (95% UI: 16,577 to 21,033) and 151,478 DALYs (95% UI: 968,605 to 1,345,776) due to MS (Wallin *et al.*, 2019).

MS is one of the world's most common neurologic disorders, and in many countries it is the leading cause of nontraumatic neurologic disability in young adults between 20 years and 40 years of age (Browne *et al.*, 2014, Filippi *et al.*, 2018*a*). For Italy, 96% and 65% of the MS patients experienced fatigue and cognitive difficulties, respectively (Battaglia *et al.*, 2017). Furthermore, the total annual costs were €22,900 at Expanded Disability Status Scale (EDSS) of 0–3, €40,100 at EDSS of 4–6.5, and €53,300 at EDSS of 7–9 (Battaglia *et al.*, 2017). The mean cost of a relapse was estimated to be €2600 (Battaglia *et al.*, 2017). MS is a very expensive disease affecting daily life and society. This illustrates the urgent need for more effective and efficient treatment options.

1.2 Causes

The causes of MS are still unknown. Previous studies have estimated that a sibling of an individual with MS has an almost 7-fold increased risk of the disease (Olsson *et al.*, 2017). The heritability of MS is polygenic and involves polymorphisms in several genes, each of which is associated with a small increase in disease risk (Filippi *et al.*, 2018*a*). Among these, genes within the HLA complex are the strongest genetic risk factors for MS (Olsson *et al.*, 2017). Specifically, the HLA class II and I genes are particularly relevant modifiers of disease risk: the class II variant HLA-DRB1*15:01 has a striking association with an increased risk of MS (odds ratio [OR] ~3), whereas the class I variant HLA-A*02 is associated with protection from the disease (OR ~0.6) (Olsson *et al.*, 2017). Beyond HLA, genome-wide association studies (GWAS) have identified ~200 genetic risk variants for MS, but each variant has a small effect on risk of disease (Filippi *et al.*, 2018*a*).

Many environmental factors are thought playing a role on the risk of MS (Filippi *et al.*, 2018*a*). Previous studies raised the argument for the influence of latitude gradient on MS (Simpson *et al.*, 2011; Olsson *et al.*, 2017). Both increased exposure to ultraviolet-B radiation and decreased vitamin D levels co-vary with latitude and show association with increased risk of MS (Simpson *et al.*, 2011, Filippi *et al.*, 2018*a*). Epstein–Barr virus (EBV) infection in adolescence and early adulthood is a well-established risk factor for MS, though the causal relationship between EBV and the disease is difficult to assess, due to many other factors linked to MS (Olsson *et al.*, 2017). Tobacco exposure through active or passive smoking is another well-known risk factor for MS: while higher amount of smoking and cumulative smoking are both associated with increased risk, low- dose oral tobacco may associated with a decreased risk of MS, as nicotine stands out as a key

candidate for such possible protection given that nicotine affects the α7 subunit of the acetylcholine receptor present on immune cells (Olsson *et al.*, 2017). Recently, adolescent obesity has been added to the list of risk factors, involved in MS pathogenesis-related inflammation pathways (Olsson *et al.*, 2017). Moreover, infectious diseases have been suggested to contribute to disease onset, with the proposed reason of generation of cross-reactive T cells and antibodies (Olsson *et al.*, 2017, Filippi *et al.*, 2018*a*). In addition, night work, over-consuming of alcohol or coffee are indicated as risk factors with weak evidence strength (Olsson *et al.*, 2017).

1.3 Pathology

The pathological hallmarks of MS are inflammation, demyelination, , neurodegeneration, glial scar formation and remyelination (Lassmann *et al.*, 2007, 2012). These pathological features are present in relapsing–remitting MS (RRMS), secondary progressive MS (SPMS) and primary progressive MS (PPMS) (Lassmann *et al.*, 2012). Inflammation in the RRMS is indicated by the infiltration of inflammatory cells into the CNS, resulting in profound damage to the blood brain barrier (BBB) (Lassmann *et al.*, 2012). However, the relationship between inflammation and damage to the BBB in PPMS and SPMS is less obvious than in RRMS (Hochmeister *et al.*, 2006). Focal lesions are most easily recognized in the WM, which harbor variables degree of inflammation, demyelination and glial reaction (Reich *et al.*, 2018). Biopsies and autopsies indicate that the earliest stages of WM demyelination, in terms of lesions, are heterogeneous and evolve over the course of months (Lucchinetti *et al.*, 2000). Recent longitudinal imaging studies suggest that lesions that form in younger people may repair more effectively (Absinta *et al.*, 2016), indicating that age strongly modulates immune-mediated regenerative processes (Ruckh *et al.*, 2012; Rawji *et al.*, 2016). Axons are preserved to a large extent, while myelin is completely lost

(Lassmann, 2018). Lesions occur on the background of inflammation, consisting of T lymphocytes, B lymphocytes, and plasma cells (Lassmann, 2018). The demyelinating process is associated with activation of astrocytes during the state of active tissue injury and the formation of gliotic scars in inactive lesions. Furthermore, MS lesions can partially become remyelinated, resulting from recruitment and differentiation of oligodendrocyte progenitor cells (Lassmann, 2018).

Normal-appearing white matter (NAWM) has been defined pathologically as macroscopically normal WM that is microscopically normally myelinated and at least 1 cm away from a plaque's edge (Filippi *et al.*, 2012). There was a lower extent of inflammation also present in the NAWM (Lassmann, 2018). Infiltration of T- and B-cells in NAWM are found (Lassmann, 2018). The brain of patients with MS also shows diffuse and global alterations, including widespread microglial activation, astrocytic gliosis, and mild demyelination and axonal loss in NAWM (Lassmann *et al.*, 2012). These changes develop, in part, independent from focal lesions (Lassmann, 2018). Once a certain threshold of axonal damage is reached in NAWM, even minor additional axonal injury will lead to worsening of the patient's neurological symptoms, owing to the exhaustion of functional compensation (Bjartmar *et al.*, 2003; Lassmann *et al.*, 2012).

The degree of inflammation, edema, microglia activation, and macrophage recruitment in GM is much less compared with that in WM (Lassmann, 2018). Demyelination in MS also involves GM (Reich *et al.*, 2018). GM demyelination can be very extensive in MS, especially in the chronic phase of the disease (Filippi *et al.*, 2019*a*). Focal demyelinated plaques are not restricted to the WM, but are also present in the cortex and deep GM (Lassmann *et al.*, 2012). GM lesions frequently show little T-cell inflammation or disruption of the BBB with leakage of plasma

proteins (Filippi *et al.*, 2019*a*). Different types of cortical lesions are found in the MS brain. Type 1 lesions are present at the cortico-subcortical border and affect the GM as well as the WM. Type 2 lesions are small perivenous intracortical lesions. Type 3 lesions do not arise from a single cortical vessel but rather appear to proceed inward from the pial surface of the brain. Subpial lesions in early MS, which are inflammatory and topographically associated with diffuse and focal leptomeningeal inflammatory aggregates (Lassmann, 2018; Reich *et al.*, 2018) , when lesions affect the entire cortex but do not pass the border between the cortex and the WM, are classified as type 4 (Lassmann, 2018).

Besides focal lesions, progressive loss of GM volume is an important feature of MS pathology, leading to massive GM atrophy (Lassmann, 2018, Filippi *et al.*, 2019*a*). GM atrophy, the degenerative processes might reflect combinations of demyelination, neurite transection, and reduced synapse or glial density (Geurts *et al.*, 2012). Mitochondrial dysfunction, abnormalities in ion channels and meningeal inflammation have been proposed as disease mechanisms in association with tissue degeneration in the cortex (Geurts *et al.*, 2012; Haider *et al.*, 2016; Lassmann, 2018). MRI studies suggest that cortical atrophy might be more closely related to diffuse neurodegeneration in the NAWM than to the extent of focal WM lesions (Mahad *et al.*, 2015). Moreover, deep GM of MS patients show diffuse neurodegeneration, which is associated with T-cell infiltration, expression of inducible nitric oxide synthase in microglia and marked accumulation of iron (Haider *et al.*, 2014).

Spinal cord lesions are a major source of clinical disability (Reich *et al.*, 2018). Demyelination affects both the WM and GM throughout the spinal cord in MS (Filippi *et al.*, 2012). GM

demyelination is more extensive and widespread throughout the spinal cord than is WM demyelination (Filippi *et al.,* 2012). Spinal cord lesions are incorporated into current MRI diagnostic criteria for MS (Thompson *et al.,* 2018). Remyelination in these lesions is variable and can depend on the presence of inflammation (Filippi *et al.*, 2012). Spinal cord atrophy results from focal inflammatory demyelination and remote neuroaxonal degeneration (Reich *et al.,* 2018). Spinal cord atrophy is most pronounced in the cervical cord, mainly resulting from loss of WM rather than GM volume (Filippi *et al.,* 2012). Surprisingly, recent finding indicates that the size of the spinal cord cross-sectional area does not predict axonal loss of the corticospinal tract (Filippi *et al.,* 2019*a*).

Optic nerve is also a major target in MS (Reich *et al.,* 2018). Loss of the contiguous retinal ganglion cells results from retrobulbar inflammatory demyelination in acute optic neuritis (Reich *et al.,* 2018). Axonal loss is assessed by optic coherence tomography, providing evidence for loss of retinal nerve fiber layer (Filippi *et al.,* 2012), possibly reflecting either subclinical inflammation of the optic nerve or retrograde trans-synaptic degeneration (Reich *et al.,* 2018). In addition, enhancement of the symptomatic lesion indicate the presence of inflammation in acute optic neuritis (Filippi *et al.,* 2012).

1.4 Clinical presentation

The clinical presentation of MS varies according to both lesion location and type of symptom onset (relapsing or progressive) (Brownlee *et al.,* 2017).

Typically, a first episode of neurological dysfunction, presumably due to RRMS, is called a clinically isolated syndrome (CIS) (Brownlee *et al.*, 2017), present in ~85% of patients (Filippi *et al.*, 2018*a*). Common CIS presentations include acute unilateral optic neuritis, partial myelitis, or brainstem syndrome (Brownlee *et al.*, 2017). Clinical features that indicate demyelination as the cause of such an episode include age younger than 40 years, an acute or subacute onset over hours to days, maximal deficit with 4 weeks of onset, and spontaneous remission (Brownlee *et al.*, 2017). In ~25% of patients, optic neuritis is the first neurological episode and is associated with a conversion to clinically definite MS between 10-15 years after clinical onset, in 34-75% of patients (Filippi *et al.*, 2018*a*).

In up to 43% of patients, sensory symptoms are the first clinical manifestation and are mainly caused by myelitis or brainstem syndromes (Filippi *et al.*, 2018*a*). Sensory symptoms include paresthesia (i.e., numbness, tingling, pins-and-needles feeling, tightness, coldness and/or swelling of the limbs or trunk), Lhermitte sign (a transient symptom presenting as an electric shock radiating down the spine or into the limbs with flexion of the neck), impairment of vibration and joint position sensation, and reduced pain and light touch perception (Filippi *et al.*, 2018*a*).

In 30-40% of patients, motor symptoms are the initial symptoms and affect almost all patients during the course of the disease (Filippi *et al.*, 2018*a*). Motor symptoms include pyramidal signs (such as Babinski sign, brisk reflexes and clonus), paresis and spasticity (Filippi *et al.*, 2018*a*). Up to 70% of patients have brainstem and cerebellar symptoms, including ocular movements impairment, oscillopsia, diplopia, ataxia, gait imbalance, dysmetria and decomposition of complex movements, slurred speech and dysphagia (Filippi *et al.*, 2018*a*). In addition, sphincter (i.e.,

urinary urgency) and sexual dysfunction often parallel the degree of motor impairment in lower extremities (Filippi *et al.*, 2018*a*).

Cognitive impairment is reported in 40-70% of patients in the early phases of disease (Rocca *et al.*, 2015). Common cognitive symptoms include impairment of information processing speed, episodic memory, attention, efficiency of information processing and executive function (Rocca *et al.*, 2015). Cognitive deficits worsen over time and affect patients' daily life activities (Rocca *et al.*, 2015), and can predict conversion from CIS to clinically definite MS (Zipoli *et al.*, 2010). Up to 95% of patients experience fatigue (Filippi *et al.*, 2018*a*). Fatigue can be associated with relapses and be a feature of daily life, presenting for years (Filippi *et al.*, 2018*a*). Affective disturbance, with depression as the most common manifestation, occurs in up to two-thirds of patients (Filippi *et al.*, 2018*a*). It is reported that up to 43% of patients can suffer from pain (trigeminal neuralgia, dysesthetic pain, back pain, visceral pain and painful tonic spasms) (Solaro *et al.*, 2004).

1.5 Diagnosis

The diagnosis of MS is primarily based on clinical criteria. The occurrence of two or more clinically distinct episodes of CNS dysfunction with at least partial resolution is sufficient for a diagnosis of RRMS (Filippi *et al.*, 2018*a*). MRI can support or replace some clinical criteria in demonstrating demyelinating lesions, as well as dissemination in space (DIS) and dissemination in time (DIT) (Filippi *et al.*, 2016*b*). MRI was formally incorporated into the diagnostic criteria of patients with CIS and suspected MS in 2001 (McDonald *et al.*, 2001). With revision for clarification and to simplify the use in the clinical setting, MRI has increased its importance in the

latest revision of the MS diagnostic criteria (the 2017 revision of the McDonald criteria) (Thompson *et al.*, 2018). Cerebrospinal fluid (CSF) examinations support a diagnosis of MS include a normal or mildly raised white cell count and protein levels, increased immunoglobulin G (IgG) index and the presence of CSF-specific IgG oligoclonal bands (OCBs) (Thompson *et al.*, 2018). CSF-specific IgG OCBs were included in the 2017 revision of the McDonald criteria (Thompson *et al.*, 2018).

Over time, the development of permanent neurological deficits and the progression of clinical disability become prominent, thus patients of this stage are classified as SPMS (Lublin *et al.*, 2014). Besides, a minority of patients have a progressive disease course from onset, which is grouped as PPMS (Lublin *et al.*, 2014).

Misdiagnosis of MS remains an issue in clinical practice (Thompson *et al.*, 2018). Careful exclusion of other neurological disorders that mimic MS is essential (Filippi *et al.*, 2018*a*). The clinician should be vigilant for the clinical and MRI "red flags" of alternative diagnosis (Thompson *et al.*, 2018), such as neuromyelitis optica spectrum disorders (NMOSDs), myelin-oligodendrocyte glycoprotein (MOG) antibody disease and cerebrovascular diseases (Filippi *et al.*, 2018*a*; Thompson *et al.*, 2018).

1.6 Treatment

Currently, 15 disease-modifying treatments (DMTs) have been approved by the Food and Drug Administration, including 5 preparations of interferon beta, 2 preparations of glatiramer acetate, monoclonal antibodies (natalizumab, alemtuzumab, daclizumab, and ocrelizumab), the

chemotherapeutic agent mitoxantrone, and the small-molecule oral agents fingolimod, dimethyl fumarate and teriflunomide (Reich *et al.*, 2018). All these DMTs are approved for RRMS, in order to reduce the likelihood of the development of new WM lesions, clinical relapses, and stepwise accumulation of disability (Reich *et al.*, 2018). Ocrelizumab is the only DMT that is approved for PPMS (Filippi *et al.*, 2018*a*).

High-dose corticosteroids is the most established treatment for MS acute relapses (Filippi *et al.*, 2018*a*). These drugs are prescribed, in order to achieve a faster functional recovery and protect against the occurrence of more severe deficits in the first weeks after treatment (Filippi *et al.*, 2018*a*). Current protocols include 3-5 days of intravenous methylprednisolone with or without oral tapering with prednisone (Filippi *et al.*, 2018*a*).

2 Role of MRI in multiple sclerosis

MRI is a particularly suitable technology for non-invasive and in-vivo evaluation of MS pathology and monitoring of disease progression and the effects of treatment, because of its high sensitivity in revealing abnormalities related to MS (Filippi *et al.*, 2019*a*).

Proton density and T2-weighted (including fluid-attenuated inversion recovery [FLAIR]) imaging are highly sensitive in detecting WM lesions in MS, enabling a prompt and accurate diagnosis of MS (Filippi *et al.*, 2012, 2019*a*). Of note, considering lesion appearance, location, and signal features with additional MRI sequences can help avoiding overdiagnosis or misdiagnosis of MS (Filippi *et al.*, 2012, 2019*a*). MS WM lesions in the brain are commonly round or ovoid and range from a few mm to more than 1cm in size, and have a high propensity to locate in the brainstem, cerebellum, and periventricular WM, which is supported by both pathological and MRI findings (Filippi *et al.*, 2012). 10-30% of T2 hyperintensities are also seen on T1-weighteed images as areas of low intensity compared with normal WM (Filippi *et al.*, 2012). T1 hypointensity is probably a consequence of marked edema and demyelination in the acute phase, while these T1 hypointensities also known as “black holes”, indicate areas with pathologically confirmed severe tissue destruction (Filippi *et al.*, 2012). Furthermore, various studies have demonstrated that the locations of WM lesions are critical for physical disability and cognitive dysfunction in MS patients (Sepulcre *et al.*, 2009; Vellinga *et al.*, 2009; Bodini *et al.*, 2011; Kincses *et al.*, 2011; Rossi *et al.*, 2012).

Diffusion tensor imaging (DTI) has been widely used for WM tractography and for estimating microstructural WM integrity, a proxy for anatomical connectivity (AC) (Alexander *et al.*, 2007). The main DTI measures are fractional anisotropy (FA), a scalar value between 0 and 1 which is a

general measure of tract integrity, axial diffusivity (AD), which is specific to axonal integrity, and radial diffusivity (RD), which is specific to myelin integrity (Alexander *et al.*, 2007). Several studies have employed DTI to demonstrate in MS patients, compared with healthy controls, altered WM microstructural integrity in terms of both lower FA and/or higher RD or AD in various brain WM regions (Roosendaal *et al.*, 2009; Enzinger *et al.*, 2015). MS WM lesions show increased MD and decreased FA with the most severe abnormalities seen in nonenhancing T1 hypointense lesions (Filippi *et al.*, 2016*a*). Beyond focal lesions, DTI is particularly suitable to quantify NAWM damage in MS. Increased MD and decreased FA have been consistently found in the NAWM of MS patients, even before the formation of new focal lesions (Filippi *et al.*, 2016*a*). Lower FA in the corpus callosum was associated with greater progression of physical disability in patients with early PPMS (Bodini *et al.*, 2013). FA and MD values of the corticospinal tract (CST) correlated with measures of locomotor disability or the pyramidal functional system score of EDSS (Wilson *et al.*, 2003; Lin *et al.*, 2005, 2007). Increased MD was found in CIS patients with motor impairment, compared with patients without pyramidal symptoms (Pagani *et al.*, 2005). More recent work have focused on the use of DTI to improve our understanding of the mechanisms related to cognitive dysfunction in MS (Enzinger *et al.*, 2015, Filippi *et al.*, 2016*a*). MS-related cognitive impairment is also associated with damage in the corpus callosum, inferior and superior longitudinal fasciculus, corticospinal tracts, forceps minor, cingulum and fornix. Cognitively impaired patients with MS show more extensive FA abnormalities than do patients without cognitive impairment (Mesaros *et al.*, 2012; Hulst *et al.*, 2013).

The extent of GM demyelination in MS varies between patients and can be widespread, especially during the chronic phase (Filippi *et al.*, 2019*a*). Limited by small size, poor contrast with the

surrounding normal-appearing GM, and partial volume effects with WM and CSF, focal cortical lesions are poorly identified using conventional MRI sequences (dual-echo T2 weighted and FLAIR) (Filippi *et al.*, 2019*a*). Though the sequences of double-inversion recovery (DIR), phase-sensitive inversion recovery (PSIR) and three-dimensional (3D) magnetization-prepared rapid acquisition with gradient echo have improved our ability to detect GM lesions (Filippi *et al.*, 2019*a*), the sensitivity of detecting cortical lesions in post-mortem study of patients with MS was only 18% (Kilsdonk *et al.*, 2016) and the inter-observer consensus of all detected cortical lesions was just 19.4% (Sethi *et al.*, 2012). Improvement of cortical lesions identification is necessary (Filippi *et al.*, 2019*a*). Cortical lesions were found in all phenotypes of MS, the number and volume of cortical lesions correlated with physical disability and cognitive impairment as well as with worsening of disability and occurrence of the progressive phase (Scalfari *et al.*, 2018).

Progressive and irreversible brain volume loss occurs in patients with MS from the early stages of the disease (Rocca *et al.*, 2017). There is loss of myelin, oligodendrocytes, and axons, whereas NAWM atrophy is likely secondary to myelin loss and axonal damage and loss (Rocca *et al.*, 2017). GM atrophy is explained predominantly by axonal loss and neuronal shrinkage, and is largely independent of demyelination (Popescu *et al.*, 2015). Quantified by T1-weighted images, the atrophy rate of 0.4% per year could be used as the cut-off to discriminate the presence or absence of 'pathological' brain volume loss with high specificity and good sensitivity (Stefano *et al.*, 2016). Although atrophy involves both WM and GM, GM atrophy provides more clinically relevant information than does WM atrophy (Rocca *et al.*, 2017). In CIS patients who had developed MS after 3 years of follow-up, progressive GM, but not WM, atrophy is seen at the baseline (Dalton *et al.*, 2004). A large-scale cross-sectional study showed that GM atrophy is slower in SPMS than in

RRMS (Roosendaal *et al.*, 2011). By contrast, WM volume in SPMS was comparable to that in RRMS (Roosendaal *et al.*, 2011). Furthermore, GM volume explained physical and cognitive impairment better than WM volume (Roosendaal *et al.*, 2011). GM atrophy can explain impairment of deteriorating cognitive function (Amato *et al.*, 2008). Besides, SPMS patients with cognitive impairment (CI) showed more severe atrophy of fronto-temporal lobes, left hypothalamus and thalami, compared with CI PPMS (Riccitelli *et al.*, 2011). A longitudinal study in MS suggested that GM atrophy is one of the key factors associated with long-term accumulation of disability and cognitive impairment in MS (Filippi *et al.*, 2013). In particular, it was demonstrated that deep GM atrophy drives disability accumulation in MS in a large-scale longitudinal study (Eshaghi *et al.*, 2018). The distribution of GM atrophy differ among different phenotypes of MS. GM atrophy start from deep GM and then extend to cortical GM for CIS and pediatric MS (Ceccarelli *et al.*, 2008; Mesaros *et al.*, 2008). In PPMS, the atrophy of cingulate cortex was involved in early stage (Eshaghi *et al.*, 2014).

In MS, functional MRI (fMRI) studies have shown that patients without CI present increased cerebral activation, more widely distributed cortical recruitment than in healthy controls, and altered functional connectivity (FC) within cognition-related regions (Rocca *et al.*, 2015). FC represents the functionally integrated synchronization (i.e., temporal relationship) among spatially separated brain regions which continuously share information with each other (van den Heuvel and Hulshoff Pol, 2010) and it may be estimated through the BOLD (blood-oxygen level dependent) signal obtained by resting-state fMRI. Resting-state fMRI studies showed reduced FC of frontal lobes in MS patients with CI (Rocca *et al.*, 2010; Bonavita *et al.*, 2011). In addition, better cognitive performance in MS patients was associated with increased FC of attention network,

supporting the adaptive role of resting-state FC alterations (Loitfelder *et al.*, 2012). FC analysis has demonstrated contradictory results. On the one hand, it was demonstrated that increased FC may be an early but finite compensatory phenomenon, which is present at the onset (CIS) and then it is subsequently lost as brain damage progresses (RRMS) (Giorgio and De Stefano, 2016). On the other hand, other studies propose that increased FC may have a "maladaptive" role, thus contributing to clinical worsening (Hawellek *et al.*, 2011).

Compared with healthy controls, MS patients showed cervical spinal cord cross-sectional area shrinkage, correlating with motor disability (Rocca *et al.*, 2011). The presence of spinal cord lesions is incorporated into current MRI diagnostic criteria for MS (Thompson *et al.*, 2018). A recent study focusing on spatial distribution of multiple sclerosis lesions in the cervical spinal cord indicated that high lesion frequency was present in patients with a more aggressive disease course, rather than long disease duration (Eden *et al.*, 2019). Furthermore, lesions located in the lateral columns and central cord area of the cervical spine may influence the clinical status in MS (Eden *et al.*, 2019).

Compared to healthy controls, MS patients with optic neuritis had a significantly reduced optic nerve radius (Harrigan *et al.*, 2017).

3 Current challenges

A number of studies have explored the association between regional GM atrophy and WM pathology. More recently, some studies have provided new, clinically relevant information by investigating non-random "patterns" of either GM atrophy (Steenwijk *et al.*, 2016; Bergsland *et al.*, 2018) or WM microstructural damage (Meijer *et al.*, 2016) through source-based morphometry (SBM). However, no study has ever assessed the relationship between non-random "patterns" of both GM atrophy and WM pathology in MS patients with mild disability, which will provide new insights on how, from relatively early disease stages, distinct spatial patterns of GM atrophy and WM microstructural damage exist and may be inter-related.

Nowadays, in the field of MS, which is the most frequent cause of non-traumatic disability in young adulthood, there is still a need to bridge the gap in linking structural and functional abnormalities in order to better clarify the complex pathogenic picture. Multimodal neuroimaging data-driven fusion approach, by searching for common information across modalities, could identify co-occurring changes across various brain measures, leveraging the cross-information of the whole dataset, and thereby being able to reveal important relationships that cannot be detected using a single modality, and thus to yield a more comprehensive picture of the multiple pathogenic mechanisms (Calhoun and Sui, 2016). To improve our understanding in MS of the intimate pathogenic mechanism of WM and GM damage in terms of coexisting brain structural and functional changes, we need to move from unimodal to multimodal fusion MRI analysis. Thus far, no study has ever employed in MS patients such methods of multimodal fusion of brain MRI data.

4 Aim of the thesis

1. To assess whether and to what extent distinct spatial patterns of GM atrophy and WM microstructural damage exist and may be inter-related, using SBM on MRI data of a MS patient cohort with relatively mild disability.

2. To uncover in MS, using multimodal MRI fusion analysis, the “hidden” relationships between brain structural damage and functional reorganization, and the shared pathophysiology across different MRI modalities from a system-level perspective.

3. To investigate clinical relevance of findings from multimodal MRI data fusion by testing their association with measures of physical disability and cognitive impairment in MS.

5 Study 1: Grey matter atrophy cannot be fully explained by white matter damage in patients with MS

Introduction

Structural abnormalities, as detected by MRI, are well known in multiple sclerosis (MS) brains in the form of grey matter (GM) atrophy and white matter (WM) damage (Geurts *et al.*, 2012, Filippi *et al.*, 2019*c*). Some studies suggested that WM damage may be spatially linked with subsequent cortical and deep GM atrophy in primary progressive and longstanding MS (Steenwijk *et al.*, 2014, 2016; Bodini *et al.*, 2016). Other studies showed that most of the cortical GM atrophy may be partially independent from the WM lesions in both early and progressive MS (Kawachi and Lassmann, 2017; Zurawski *et al.*, 2017).

Few recent studies have revealed in MS, at the level of "patterns" (i.e., co-varying structurally and/or functionally related regions of the human brain), the presence of GM atrophy (Steenwijk *et al.*, 2016; Bergsland *et al.*, 2018) or WM microstructural damage (Meijer *et al.*, 2016), as expressed by low fractional anisotropy (FA) on diffusion tensor imaging (DTI) data. Such patterns were detected with source-based morphometry (SBM), a novel model-free and data-driven multivariate MRI-based approach using independent component analysis (ICA) on brain images of different MRI modalities (Xu *et al.*, 2009). SBM allows grouping brain structural abnormalities into spatial patterns, well beyond the traditional assessment of single brain regions(Gupta *et al.*, 2015). Such approach may thus help shed light on complex pathogenic mechanisms, including possible relationships between GM atrophy and WM microstructural damage in distinct anatomical regions of the MS brain. Given the great potential of this approach in providing new insights on this relevant issue, we used here SBM on MRI data of a MS patient cohort with relatively mild disability in order to assess whether and to what extent distinct spatial patterns of GM atrophy and

WM microstructural damage exist and may be inter-related. To increase the reliability of the results, the same procedure was performed on an independent MRI dataset with similar characteristics.

Methods

Participants

Two independent subject datasets were recruited, respectively, before and after MR scanner upgrade (Table 1): the "Study dataset" of 41 MS patients and 28 normal controls (NC), and the "Reliability dataset" of 39 MS patients and 13 NC. All MS patients were diagnosed with 2010 McDonald criteria (Polman *et al.*, 2011) and had to be free from relapses and corticosteroid treatment for at least 1 month before study entry. NC were recruited among laboratory and hospital workers, had normal neurological examination and no history of neurological disorder. A full description of the "Study dataset" and "Reliability dataset" can be found in Table 1.

In MS patients, disability was measured on the Expanded Disability Status Scale (EDSS) (Kurtzke, 1983) whereas cognition was assessed by a trained and blinded neuropsychologist, using the Brief Repeatable Battery (BRB) (Rao, 1990). Failure of a BRB test was defined as a score < 2 standard deviations from the Italian normative values (Amato *et al.*, 2006) and cognitive impairment was defined as a failure of ≥2 BRB tests.

The study protocol received approval from the Ethics Committee of Azienda Ospedaliera Universitaria Senese. Informed written consent was obtained from all participants before study entry in accordance with Declaration of Helsinki.

Table 1. Demographic, clinical and LV characteristics of the study groups. Study and Reliability datasets were acquired, respectively, before and after MR scanner upgrade

	Study Dataset (41 MS, 28 NC)	*Reliability dataset (39 MS, 13 NC)*	*p-value*
Age (mean±SD, years)			
MS (41 RRMS)	35.6 ± 10.4	40.7 ± 9.1	0.020[a]
NC	33.2 ± 10.0	35.6 ± 8.9	0.087[a]
p-value (MS v NC)	0.348[a]	0.257[a]	
Sex (male/female number)			
MS (35 RRMS, 3 SPMS, 1 PPMS)	13/28	13/26	0.877[b]
NC	5/23	6/7	0.057[b]
p-value (MS v NC)	0.198[b]	0.406[b]	
Disease duration (mean±SD, years)	9.1 ± 7.0	8.0 ± 8.0	0.514[c]
EDSS (median [range])	1.5 (0-6)	1.5 (1-6.5)	0.661[c]
Cognitive impairment (yes/no) [%]	9/32 [22%]	12/27 [31%]	0.370[c]
WM LV (median [range], cm^3)	5.61 (0.30-79.05)	3.80 (0.14-31.86)	0.072[c]
Projection (median [range], cm^3)	3.4 (0.22-32.39)	2.38 (0.04-15.19)	-
Association (median [range], cm^3)	0.33 (0-9.28)	0.27 (0-2.09)	-
Commissural (median [range], cm^3)	1.19 (0.06-9.35)	0.62 (0-5.73)	-
Subcortical (median [range], cm^3)	1.74 (0.09-33.25)	1.87 (0-13.94)	-
Brainstem/cerebellar (median [range], cm^3)	0.09 (0-1.51)	0.08 (0-0.74)	-

[a]Two-sample t-test

[b]Chi-squared test

[c]Mann-Whitney U test

RRMS: relapsing-remitting multiple sclerosis; SPMS: secondary progressive multiple sclerosis; PPMS: primary progressive multiple sclerosis.

See text for abbreviations

MRI data acquisition

MRI data were acquired with an 8-channel head coil on a 3 Tesla MR scanner (Philips Medical Systems, Best, The Netherlands) located at Meyer University Hospital, Florence. A sagittal survey image was used to identify anterior and posterior commissures. Sequences were acquired in the axial plane parallel to the bicommissural line. A dual-echo, turbo spin-echo sequence (repetition time [TR]/echo time [TE]1/TE2 = 4000/10/100 ms, voxel size = 1×1×3 mm) yielded proton density (PD) and T2-weighted (T2-W) images. DTI data were an echo-planar imaging sequence (TR = 7036 ms; TE = 196 ms; voxel size = 2.5 mm^3) with 32 diffusion directions and b-value = 900 s/mm^2. A high-resolution T1-weighted image (T1-W, TR = 10 ms, TE = 4 ms, voxel size = 1 mm^3) was also acquired for image registration, anatomical mapping and analysis of GM volumes. Study and Reliability datasets were acquired, respectively, before and after MR scanner upgrade and using the same imaging protocol.

MRI data analysis

It was performed at the Quantitative Neuroimaging Laboratory (QNL) of the University of Siena. All images were visually assessed to rule out artifacts or incidental findings.

White matter lesions

MS lesions were outlined on PD images by an experienced observer (RTB), blinded to patient identity, with a semiautomated segmentation technique based on user-supervised local

thresholding (Jim 6.0, Xinapse System, Leicester, UK) which allowed compute global lesion volume (LV) across brain.

Regional LV was computed using the WM parcellation map (WMPM) of a John Hopkins University (JHU) standard-space atlas (Eve Atlas, www.mristudio.org). First, for each patient LV was calculated in each WM region (label) of the atlas by masking WMPM with the corresponding lesion mask (Oishi *et al.*, 2009). Then, WM regions were grouped in 5 anatomically meaningful areas, such as projection, association, commissural, subcortical and brainstem/cerebellar WM, in line with previous studies (Hua *et al.*, 2008), and for each area LV was computed by summing the values from all corresponding WM regions (Table 2).

Binarized lesion mask of each patient was registered onto MNI152 standard brain through tools of FSL (FMRIB Software Library, www.fmrib.ox.ac.uk/fsl) using linear registration (FLIRT [FMRIB Linear Image Registration Too]) (Jenkinson and Smith, 2001) followed by nonlinear registration (FNIRT [FMRIB Non-linear Image Registration Tool]) (Andersson *et al.*, 2007). Two experienced observers (JZ and AG) independently checked all lesion masks registered onto standard brain and an agreement was found in all cases. Finally, lesion probability map (LPM) was generated first merging and then averaging all lesion masks previously registered onto standard brain.

Table 2. Regions of the WM groups used for calculation of regional LV

White matter group	*Regions*

Projection WM	Cerebral peduncle, internal capsule (anterior and posterior limbs, retrolenticular part), posterior thalamic radiation, corona radiata (anterior, superior and posterior), sagittal stratum
Association WM	Superior longitudinal fascicle, superior fronto-occipital fascicle, inferior fronto-occipital fascicle, external capsule, uncinate fascicle, cingulum, fornix, stria terminalis
Commissural WM	Corpus callosum (genu, body, splenium), tapetum
Subcortical WM	Superior parietal, frontal (superior, middle, inferior), precentral, postcentral, angular, pre-cuneus, cuneus, lingual, fusiform, occipital (superior, inferior, middle), temporal (superior, inferior, middle), supramarginal, fronto-orbital (lateral, middle), rectus
Brainstem/Cerebellar WM	Corticospinal tract, cerebellar peduncle (superior, inferior, middle), medial lemniscus, pontine crossing tract, cerebellar white matter

See text for abbreviations

Grey matter preprocessing

We followed the VBM (voxel-based morphometry) pipeline of SPM12 (Statistical Parametric Mapping, http://www.fil.ion.ucl.ac.uk/spm/). On T1-W images, GM segmentation was performed using the Unified Segmentation method after "filling" hypointense lesions (Battaglini *et al.*, 2012). Then, DARTEL (Diffeomorphic Anatomical Registration using Exponentiated Lie algebra) was used to determine the nonlinear deformations for image warping and to increase the accuracy of inter-subject alignment. Finally, all GM images were spatially normalized to MNI standard brain and smoothed with a 8 mm-full width at half maximum (FWHM) Gaussian kernel, thus representing GM concentration, a proxy for GM volume.

White matter preprocessing

DTI data were preprocessed through the FSL program *Eddy*, which corrects for eddy current-induced distortions, subject movement and signal dropout. Then, we used FDT (FMRIB Diffusion Toolbox) to obtain FA images by fitting a diffusion tensor model at each voxel. All subjects' FA images were first registered onto a standard-space image (FMRIB58_FA) using FNIRT (Smith *et al.*, 2006) and then smoothed with a 3 mm-sigma (i.e., 7 mm-FWHM) Gaussian kernel. For each MS patient, the information on lesion mask was incorporated into the FNIRT step in order to avoid over-distortion of lesion areas.

Source-based morphometry of grey matter and fractional anisotropy images

Following the original pipeline (Xu *et al.*, 2009), analyses were performed on images of GM concentration (Gupta *et al.*, 2015) (i.e., without modulation by Jacobian determinant) and FA of the Study dataset using GIFT (Group ICA of FMRI Toolbox; http://mialab.mrn.org/software/gift/). The number of IC (i.e., patterns) was automatically estimated with the "minimum description length" criterion through a neural network algorithm (Infomax). The statistical reliability of these patterns was tested by using ICASSO (software for investigating the reliability of ICA estimates by clustering and visualization), which repeated estimation 10 times with different initial conditions and bootstrapped datasets. For each time of estimation, a set of IC was obtained from bootstrapped samples of the image series. Each bootstrapped dataset consisted of about one third of the total images in the series.

Patterns were arrayed into 2 matrices. The first matrix was a "mixing matrix" (subject-by-pattern), which indicates the loading coefficient of each subject for each pattern. The value of the subject-

wise loading coefficient represents the corresponding GM/FA pattern (i.e., source), and can be viewed as the degree to which a pattern is present in a subject. A lower loading coefficient of the GM and FA patterns represents, respectively, GM atrophy and microstructural damage along WM tracts. The second matrix was a "source matrix" (pattern-by-GM/FA voxels), which reflects the relationship between the pattern and the GM/FA voxels.

Statistical analysis

Differences between MS and NC were tested, using the mixing matrix's loading coefficients of each pattern, with a general linear model, adjusted for age and sex. Statistical threshold was $p<0.05$, False Discovery Rate (FDR)-corrected for multiple comparisons (Winkler *et al.*, 2016).

In order to extract vectors (i.e., variables) for subsequent multivariate regression models, the source matrix of each pattern showing group difference was converted into Z scores and thresholded>3, thus creating a "pattern mask". Then, the mean of the voxels within the "pattern mask" was calculated for each patient, generating a $N_{subj} \times 1$ vector for each pattern, in line with a recent pipeline (Sui *et al.*, 2018).

Spearman coefficient was used to compute correlations between measures of GM (i.e., vectors of GM atrophy patterns) and WM (i.e., vectors of FA patterns, global and regional LV), FDR-corrected for multiple comparisons.

We then used stepwise multivariate linear regression analyses, in which vectors of each GM atrophy pattern were treated as dependent variable while FA pattern vectors, global LV (log-

transformed to allow normal distribution) and regional LV (Z-transformed to allow normal distribution) were considered as independent variables while age, sex and disease duration as covariates. Of note, only MRI measures showing significant Spearman correlation will be included in the regression model. The combination of measures of WM macro- and microstructural damage able to best predict each pattern of GM atrophy in the Study dataset was tested using the following equation:

$$\text{GM atrophy Pattern} = \text{Constant} + \beta_1 \times (\text{Regional LV}) + \beta_2 \times (\text{FA Pattern})$$

Finally, to increase reliability of the results, the same SBM procedure was repeated on an independent dataset of MS patients and NC with similar characteristics. First, SBM was run on GM and FA images of the Reliability dataset, using the same setting as the Study dataset. Second, the multivariate regression model (i.e., Beta-coefficients) best predicting each GM atrophy pattern of the Study dataset was applied to the Reliability dataset. Pearson correlations between true and predicted values of each GM atrophy pattern were assessed.

P-value <0.05 was set as significant for all analyses, performed with R software (https://www.r-project.org/).

Results

Clinical, demographic and LV characteristics of the study groups

There was no age and sex difference between MS and NC for both Study (p=0.348 and p=0.198, respectively) and Reliability (p=0.257 and p=0.406, respectively) datasets. In the comparison between Study and Reliability datasets, there was no age and sex difference for NC (p=0.087 and p=0.057, respectively) and MS patients did not differ for sex (p=0.877), disease duration (p=0.514), EDSS (p=0.661), proportion of cognitive impairment (p=0.370) and LV (p=0.072). Data are summarized in Table 1.

Grey matter patterns

Six GM patterns were automatically detected across brain of the Study dataset.

GM atrophy (p<0.05, FDR-corrected) was found in MS patients compared to NC for Pattern-1 ("deep GM pattern": caudate and thalamus), Pattern-2 ("sensorimotor GM pattern": paracingulate gyrus, precuneous cortex, precentral gyrus, supplementary motor cortex, superior frontal gyrus and postcentral gyrus) and Pattern-4 ("posterior GM pattern": inferior temporal gyrus, occipital fusiform gyrus, lingual gyrus, posterior cingulate and precuneous cortex) (Figure 1 A-B, Table 3). No significant group differences were found for Pattern-3 (inferior frontal gyrus, pars opercularis), Pattern-5 (lateral occipital cortex, parahippocampal gyrus) and Pattern-6 (cerebellar cortex).

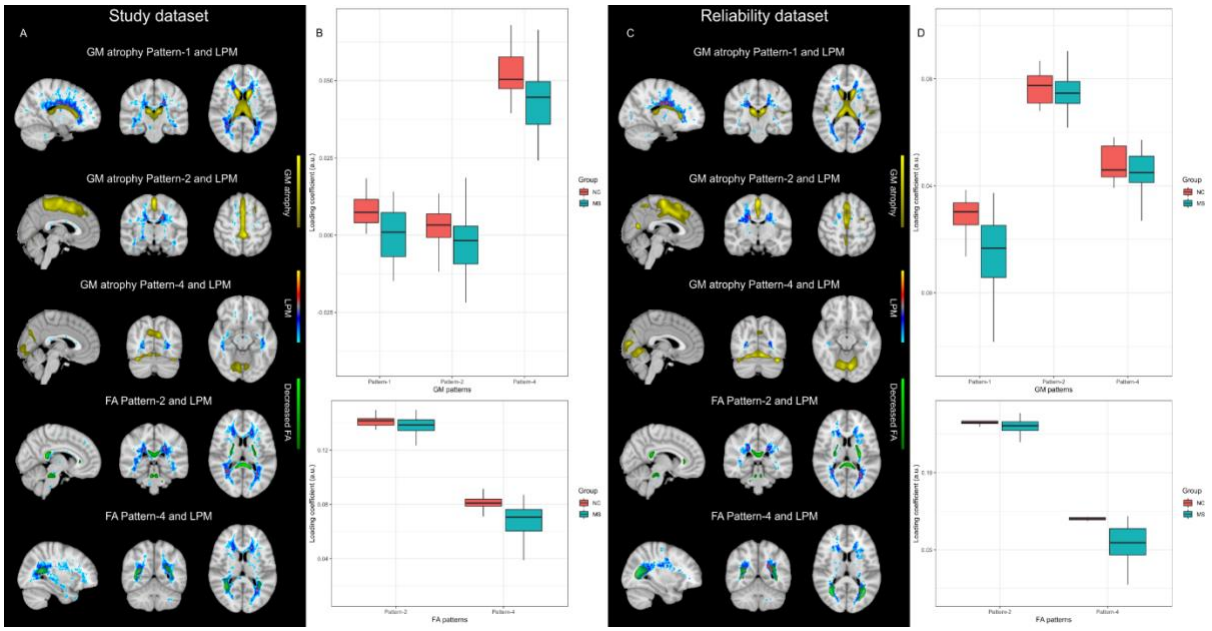

Figure 1. Significant patterns of GM atrophy (in yellow, Z>3) and WM microstructural damage (i.e., decreased FA) (in green, Z>3) in our group of MS patients with relatively mild disability compared to NC and corresponding box-plots of loading coefficients are shown for the Study (A and B) and Reliability (C and D) datasets. Lesion probability map (in light-blue to red, range: 1-46% for both datasets) is also shown to assess the spatial relationship between lesions and significant patterns. Background image is the MNI152 standard brain, in radiological orientation. See text for abbreviations; a.u.: arbitrary unit.

Table 3. Patterns of GM atrophy (p<0.05, FDR-corrected) in MS patients with relatively mild disability compared to NC in the Study dataset

GM atrophy pattern	*Brain region (local maxima)*	*Side*	*MNI (x, y, z)*	*Z-value*	*P-value of pattern*

1	Caudate	R	12, 18, 10	8.8	0.006
		L	-12, 14, 12	9.1	
	Thalamus	L	-8, -18, 16	8.1	
		R	10, -20, 16	7.7	
2	PCG	R	2, 12, 48	7.2	0.014
	PreCC	L	-6, -36, 48	4.9	
	PreG	L	-2, -38, 54	7.7	
	SMC	M	0, 6, 54	6.9	
	PreCC	R	2, -38, 56	6.9	
	SFG	R	4, 14, 56	5.7	
	PosG	L	-4, -44, 66	5.5	
		R	6, -46, 66	4.6	
4	ITG	L	-46, -54, -26	5.6	0.001
	OFG	R	18, -80, -18	4.7	
	LG	R	10, -68, -12	4.5	
	PosC	M	0, -63, 15	3.6	
	PreCC	L	-10, -72, 28	5.3	
		R	8, -72, 34	4.6	

Within each pattern, brain regions were ordered by increasing coordinates on the z-axis

Abbreviations

FDR: false discovery rate; L: left; R: right; PCG: paracingulate gyrus; PreCC: precuneous cortex; PreG: precentral gyrus; SMC: supplementary motor cortex; SFG: superior frontal gyrus; PosG: postcentral gyrus; ITG: inferior temporal gyrus; OFG: occipital fusiform gyrus; LG: lingual gyrus; PosC: posterior cingulate.

Fractional anisotropy patterns

Four FA patterns were automatically detected across brain of the Study dataset.

Lower FA (p<0.05, FDR-corrected) in MS than NC was found for FA Pattern-2 (corticospinal tract [CST, internal capsule and brainstem] and splenium of the corpus callosum [sCC], both mainly in the normal appearing WM) and FA Pattern-4 (posterior thalamic radiation [PTR] and corona radiata [PCR], overlapping with WM lesions) (Figure 1 A-B, Table 4).

No significant group difference was found for FA Pattern-1 (superior corona radiata). FA Pattern-3 was visually identified as noise and thus discarded.

Table 4. Patterns of decreased FA (p<0.05, FDR-corrected), reflecting microstructural damage along WM tracts, in MS with relatively mild disability compared to NC in the Study dataset

FA pattern	*Brain region (local maxima)*	*Side*	*MNI (x, y, z)*	*Z-value*	*P-value of pattern*
2	CST	L	-23, -15, 9	3.6	0.023
	Splenium of CC	L	-6, -39, 15	4.8	
		R	10, -40, 17	4.7	
4	PTR/OR	L	-38, -51, 4	3.9	< 0.001
		R	33, -50, 15	5.5	
	PCR	L	-27, -46, 22	4.4	

Within each pattern, brain regions were ordered by increasing coordinates on the z-axis

Abbreviations
FA: fractional anisotropy; FDR: false discovery rate; L: left; R: right; CST: corticospinal tract; CC: corpus callosum; PTR: posterior thalamic radiation; OR: optic radiation; PCR: posterior corona radiata.

Correlation between patterns of grey matter atrophy and white matter damage measures

The anatomical relationship between GM atrophy patterns and lesions across brain (LPM) is shown in Figure 1. The three GM atrophy patterns showed a moderate-to-close-correlation with the two FA patterns (Figure 2) and with global and supratentorial LV (Table 5A).

The stepwise multivariate linear regression analysis (Table 5B) showed that GM atrophy Pattern-1 was highly explained (R_2=0.723, adjusted [for the number of predictors] R_2=0.709, p<0.001) by both LV along WM projection tracts and FA Pattern-4; GM atrophy Pattern-2 was moderately explained (R_2 = 0.522, adjusted R_2 = 0.510, p<0.001) by FA Pattern-4; finally, GM atrophy Pattern-4 was moderately explained (R_2 = 0.604, adjusted R_2 = 0.584, p<0.001) by both LV in subcortical WM and FA Pattern-4.

Table 5. Correlation between patterns of GM atrophy and measures of WM damage (A) and stepwise multivariate linear regression models (B) in the Study dataset

	GM atrophy Pattern-1		***GM atrophy Pattern-2***		***GM atrophy Pattern-4***	
A: Spearman correlation						
	Rho	*p-value**	*Rho*	*p-value**	*Rho*	*p-value**
FA Pattern-2	0.54	<0.001	0.57	<0.001	0.65	<0.001
FA Pattern-4	0.67	<0.001	0.70	<0.001	0.73	<0.001
Global LV	-0.77	<0.001	-0.66	<0.001	-0.64	<0.001
Projection LV	-0.73	<0.001	-0.60	<0.001	-0.61	<0.001
Association LV	-0.59	<0.001	-0.55	<0.001	-0.65	<0.001
Commissural LV	-0.67	<0.001	-0.52	<0.001	-0.56	<0.001
Subcortical LV	-0.71	<0.001	-0.63	<0.001	-0.65	<0.001
Brainstem/Cerebellar LV	-0.33	0.038	-0.37	0.018	-0.55	<0.001
B: Multivariate regression model						

	R_2 = 0.723[a]*, Adj. R_2 = 0.709, RMSE = 0.044	R_2 = 0.522[a]*, Adj. R_2 = 0.510, RMSE = 0.053	R_2 = 0.604[a]*, Adj. R_2 = 0.584, RMSE = 0.045
	Beta coefficient	*Beta coefficient*	*Beta coefficient*
Constant	0.178	0.048	0.432
Predictors			
FA Pattern-4	0.566[b]	1.005[a]	0.524[b]
Projection LV	-	-	-
	0.041[b]		
Subcortical LV	-	-	0.524[b]

Adj.: adjusted for the number of predictors, RMSE: root mean square error

*FDR (False Discovery Rate)-corrected

[a]p<0.001

[b]p<0.05

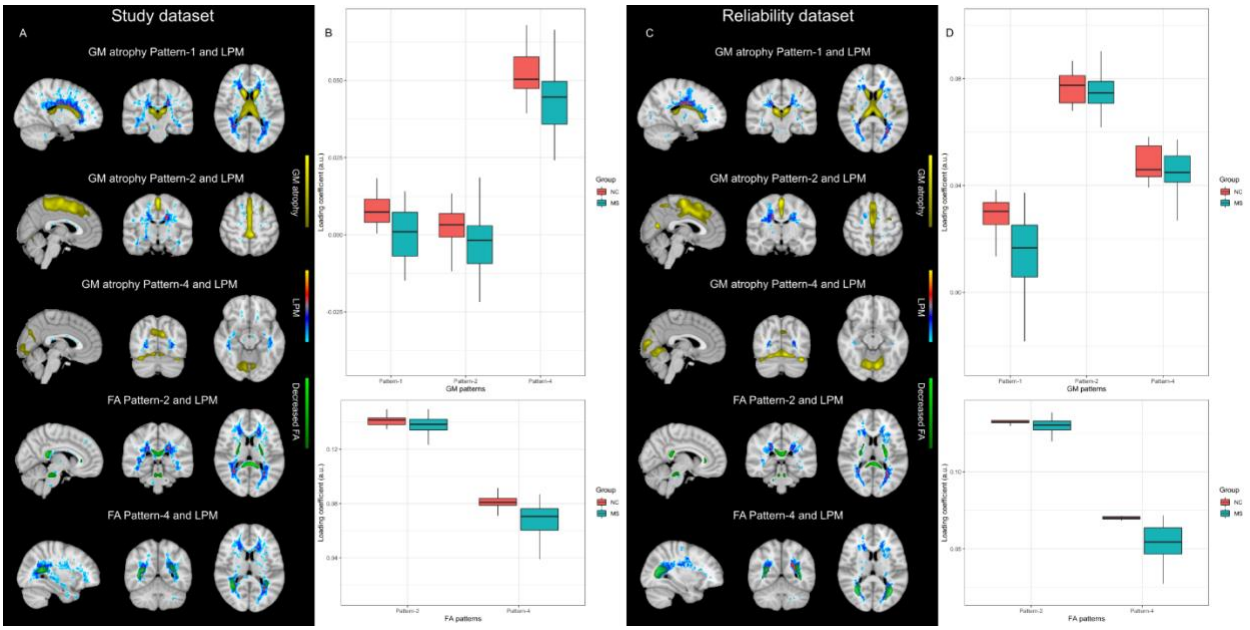

Figure 2. Spatial relationship between patterns of GM atrophy (in yellow. Z>3) and WM microstructural damage (i.e., decreased FA) (in green, Z>3) in our group of MS patients with relatively mild disability for the Study (left panel) and Reliability (right panel) datasets. Background image is the MNI152 standard brain, in radiological orientation. See text for abbreviations

Generalizability of source-based morphometry and multivariate regression model

When the analysis was performed on the Reliability dataset, we found high spatial similarity with corresponding patterns of the Study dataset (Figure 1C-D, Tables 6 and 7). As shown in (Figure 3), all predicted values of GM atrophy patterns in the Reliability dataset showed significant correlations with corresponding true vales of the Study dataset (GM atrophy Pattern-1: r=0.77, p<0.001; GM atrophy Pattern-2: r=0.60, p<0.001; GM atrophy Pattern-4: r=0.58, p<0.001), suggesting good generalizability of the multivariate regression models (Sui *et al.*, 2018).

Table 6. Patterns of GM atrophy (p<0.05, FDR-corrected) in MS patients with mild disability compared to NC in the Reliability dataset

GM atrophy pattern	*Brain region (local maxima)*	*Side*	*MNI (x, y, z)*	*Z-value*	*P-value of pattern*
1	Caudate	R	13, 21, 4	7.8	0.004*
		L	-12, 18, 7	8.1	

	Thalamus	L	-9, -23, 15	8.1	
		R	10, -21, 15	8.6	
2	CG	R	3, 6, 41	4.4	0.787
		L	-3, 2, 44	4.7	
	SFG	R	4, 20, 50	4.1	
		L	-3, 19, 52	4.4	
	SMC	R	3, -9, 53	4.6	
		L	-1, -9, 60	4.4	
4	OFG	L	-18, -84, -20	5.8	0.787
		R	24, -72, -17	5.0	
	LG	L	-7, -71, -12	5.9	
		R	7, -61, -6	5.6	
	CC	L	-2, -84, 10	4.6	
		R	2, -84, 11	5.4	
	PosC	M	0, -65, 17	3.1	
	MTG	R	40, -67, 18	3.9	

Within each pattern, brain regions were ordered by increasing coordinates on the z-axis

Abbreviations

FDR: false discovery rate; L: left; R: right; CG: cingulate gyrus; SFG: superior frontal gyrus; SMC: supplementary motor cortex; OFG: occipital fusiform gyrus; LG: lingual gyrus; CC: cuneal cortex; PosC: posterior cingulate; MTG: middle temporal gyrus.
*GM atrophy in MS patients compared with NC

Table 7. Patterns of decreased FA (p<0.05, FDR-corrected), reflecting microstructural damage along WM tracts, in MS with mild disability compared to NC in the Reliability dataset

FA pattern	*Brain region (local maxima)*	*Side*	*MNI (x, y, z)*	*Z-value*	*P-value of pattern*
2	CST	L	-25, -18, 9	3.7	0.044*
	Splenium of CC	L	-2, -37, 16	4.5	
		R	11, -39, 20	4.4	
4	PTR/OR	R	32, -60, 14	6.3	< 0.001*
		L	-32, -63, 15	5.9	

Within each pattern, brain regions were ordered by increasing coordinates on the z-axis
Abbreviations
FA: fractional anisotropy; FDR: false discovery rate; L: left; R: right; CST: corticospinal tract; CC: corpus callosum; PTR: posterior thalamic radiation; OR: optic radiation.
*decreased FA in MS patients compared with NC

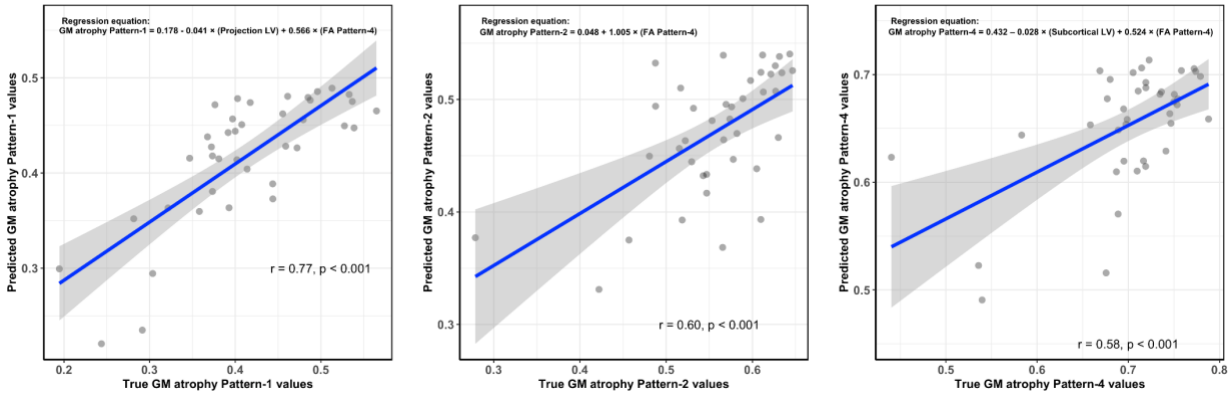

Figure 3. Scatter-plots showing correlation between predicted values of GM atrophy pattern in the Reliability dataset and corresponding true values obtained from multivariate regression analyses in the Study dataset.

Discussion

In this study, we sought to assess in MS patients with relatively mild disability whether and to what extent distinct anatomical non-random "patterns" of GM atrophy and WM microstructural damage may be inter-related. For this purpose, we applied to MRI data SBM, a novel model-free and data-driven multivariate approach using spatial ICA.

Non-random patterns of grey matter atrophy and white matter microstructural damage

Most of the GM regions of our atrophy patterns were found in a recent longitudinal SBM study on MS (Bergsland *et al.*, 2018), whose atrophy patterns indeed included caudate and thalamus (GM atrophy Pattern-1), precuneous cortex, precentral gyrus, supplementary motor cortex (GM atrophy Pattern-2), inferior temporal gyrus and lingual gyrus (GM atrophy Pattern-4). Moreover, our

atrophy pattern in the posterior GM was in line with another recent SBM study on longstanding MS, where a pattern of cortical thinning similarly mapped on lingual gyrus and posterior cingulate cortex (Steenwijk *et al.*, 2016).

As for FA patterns, decreased FA in CST, sCC (FA Pattern-2) and PTR (FA Pattern-4) was also found in a recent SBM study on secondary progressive MS (Meijer *et al.*, 2016). However, in that study sCC and CST mapped in separate patterns, thus demonstrating that WM microstructural damage may be differently organized in MS groups with different disability.

Despite similarities, differences across SBM studies exist and may be related to patient populations as well as methodologies, including MR field strength, type of SBM and pattern detection (automated vs. predefined). Interestingly, however, in the present study the three significant GM atrophy patterns and the two FA patterns in the Study dataset were confirmed, with high spatial similarity, on the Reliability dataset, suggesting that such patterns are stable and consistent when using the same methodology.

Atrophy in caudate and thalamus, expressed here as DGM pattern (GM atrophy Pattern-1), was recently shown to drive disability worsening in MS (Eshaghi *et al.*, 2018) and is likely due to demyelination, inflammation, axonal injury, iron deposition and oxidative stress (Haider *et al.*, 2014). Atrophy found in sensorimotor cortex (GM atrophy Pattern-2), despite relatively mild disability, was found associated with motor dysfunction (Sailer *et al.*, 2003, Bodini *et al.*, 2009*b*; Prinster *et al.*, 2010; Narayana *et al.*, 2012). Atrophy in posterior cortex (GM atrophy Pattern-4)

was similarly found in a recent SBM study (Steenwijk *et al.*, 2016), which linked it to impairment in information processing speed.

Reduced FA in our MS group with relatively mild disability was found in CST and sCC (FA Pattern-2), in line with a previous tract-based spatial statistics study where both tracts resulted associated with EDSS in MS patients with mild disability (Giorgio *et al.*, 2010). Moreover, reduced FA was found in PCR and PTR (FA Pattern-4). The former, containing descending projection fibers of the CST, subserves motor function to the lower limbs. Altered diffusion in PCR is in line with a recent study on pediatric-onset MS in the early adulthood with no or minimal disability (Giorgio *et al.*, 2017) and highlights that, even at this disease stage, there is already damage along a WM tract clinically eloquent for ambulation, which indeed represents the major contributor to EDSS. The latter, also containing projection fibers, is an important cognition-related WM tract in MS, showing close associations with processing speed and visual working memory (Yu *et al.*, 2012).

Association between patterns of grey matter atrophy and measures of white matter damage

The three significant GM atrophy patterns showed a moderate-to-close relationship with FA, particularly in the posterior WM regions overlapping lesions (FA Pattern-4). Moreover, they also correlated with both global and regional LV. Most of these associations with supratentorial LV were particularly close for caudate and thalamus atrophy (GM atrophy Pattern-1), thus supporting the idea that WM lesions are an important contributor to atrophy in these structures (Steenwijk *et al.*, 2014). Indeed, in both Study and Reliability datasets, the multivariate regression model showed

that atrophy in caudate and thalamus (GM atrophy Pattern-1) was highly explained, in the order of 70%, by lesion load along WM projection tracts and decreased FA in PCR and PTR (FA Pattern-4). This finding highlights the importance of WM damage, in terms of both macrostructural damage along WM tracts clinically eloquent for motor function and WM microstructural damage in posterior regions mostly overlapping with lesions, to the occurrence of DGM atrophy.

Interestingly, however, cortical atrophy (GM atrophy Pattern-2 and -4) was less explained by WM damage (in the order of about 50% in the two datasets) thus indicating that this may be, at least in part, independent from WM damage in MS patients with relatively mild disability. The remaining variance might be explained by other pathological processes, including meningeal inflammatory infiltrates, recently shown to act as independent factor for cortical atrophy beyond WM lesions [6,32].

Strengths and Limitations

Important limitations of this study lie in the cross-sectional design and the relatively small sample size. Compared to VBM, surface-based methods may potentially yield a better registration quality (Steenwijk *et al.,* 2016). However, they do not include in the default pipeline important brain structures for MS such as deep GM regions and cerebellum (Steenwijk *et al.*, 2016) and do not automatically estimate the number of independent components in SBM, thus potentially introducing a bias. We are aware that VBM-based nonlinear registration may, to some extent, be affected by the presence of brain atrophy. Reassuringly, a careful check of all registered images allowed us to rule out the presence of clear misregistrations affecting the creation of brain patterns. Moreover, the great reproducibility of our results in two independent datasets with similar characteristics strongly increases the confidence in the robustness of the study.

SBM was applied here to assess patterns of GM atrophy and WM microstructural damage and their inter-relation. This approach has shown some strengths, as it seems to ideally overcome some limitations of graph theory-based structural network analysis regarding inappropriately defined "nodes" through atlas-based parcellation, arbitrarily thresholded correlation matrix and high degree of abstraction of network matrix, whose complex measures are simply represented by numbers (Xu *et al.*, 2009; Smith, 2012). Moreover, ICA-based analyses, including SBM, turn out be more straightforward to interpret compared to canonical correlation analysis (CCA) due to the clear distinction of correlation coefficients (Calhoun and Sui, 2016), adjustment for the nuisance effect of the dependence between variables (Lee *et al.*, 1999) and automated estimation of the independent component number (Li *et al.*, 2007). However, SBM performs a separate assessment of the GM atrophy and FA patterns and the subsequent post-hoc analyses of correlations and multivariate regression. Future studies should assess the pathogenic relevance of the direct combination or "fusion" of such patterns using upfront imaging analysis methods.

In conclusion, by using cutting-edge MR-based methodology, we provide here evidence of a close link between WM damage and DGM atrophy. By contrast, cortical atrophy seems to be, at least in part, independent from WM damage. This could be explained by a primary cortical neurodegeneration and perhaps related to other primary mechanisms, including meningeal inflammation. Further studies should be performed to shed more light on this clinically relevant aspect of the MS pathophysiology.

Summary

Background: Various studies explored the association between regional grey matter (GM) atrophy and white matter (WM) pathology in MS patients. More recently, source-based morphometry (SBM) was used to assess non-random "patterns" of GM atrophy or WM microstructural damage. Objective: To assess whether and to what extent such patterns may be inter-related in MS patients with relatively mild disability.

Methods: SBM was applied to images of GM concentration and fractional anisotropy (FA), in MS patients (n=41) with relatively mild disability (median EDSS=1) and normal controls (NC, n=28). The same SBM procedure was repeated on an independent and similar dataset (39 MS patients and 13 NC).

Results: We found in MS various patterns of GM atrophy and reduced FA ($p<0.05$, corrected). Deep GM atrophy was mostly (70%) explained by lesion load in projection tracts and lower FA in posterior corona radiata and thalamic radiation. By contrast, sensorimotor and posterior cortex atrophy was less (50%) dependent from WM damage. The reliability analysis showed similar results.

Conclusion: In relatively early MS, we found a close link between deep GM atrophy pattern and WM damage while patterns in sensorimotor and posterior cortex seems to be partially independent from WM damage and perhaps related to primary mechanisms.

6 Study 2: Linked structural and functional brain abnormalities in patients with multiple sclerosis

Introduction

Several MRI studies have demonstrated that the brain of multiple sclerosis (MS), a widespread inflammatory, demyelinating and neurodegenerative disease of the central nervous system (Filippi *et al.*, 2018*a*), encompasses multiple structural abnormalities, in the form of grey matter (GM) atrophy (Rocca *et al.*, 2017), macroscopic white matter (WM) lesions and microstructural damage (Enzinger *et al.*, 2015, Filippi *et al.*, 2019*a*) as well as functional connectivity (FC) abnormalities (Rocca *et al.*, 2015; Filippi *et al.*, 2017). However, there is still need to bridge the gap in linking such structural and functional changes. Indeed, they have always been separately shown in MS using single MRI modalities. Integrating such modalities might provide a more comprehensive view of the MS complex pathogenic scenario (Rocca *et al.*, 2015, Filippi *et al.*, 2018*b*) by revealing important "hidden" relationships that might go undetected using unimodal MRI studies (Calhoun and Sui, 2016).

Linked independent component analysis (ICA), a multimodal neuroimaging data-driven fusion approach, by looking for common and shared information across modalities, may identify co-occurring and linked changes across brain (Groves *et al.*, 2011; Wolfers *et al.*, 2017, Llera *et al.*, 2019*a*). Thus far, linked ICA has been employed in MRI studies to assess covariance across structural modalities in aging (Douaud *et al.*, 2014), neuropsychiatric disorders (Wolfers *et al.*, 2017; Alnæs *et al.*, 2018) and across structural and functional modalities in neuropsychiatric and traumatic brain disorders (Manning *et al.*, 2019; Wu *et al.*, 2019).

Based on this background, in order to "uncover" for the first time in MS the shared pathogenic mechanisms of brain tissue injury and functional re-organization, we applied linked ICA to images of GM density, WM microstructure and functional brain networks.

Material and methods

Study subjects

We included 100 relapsing-remitting (RR) MS patients and 43 normal controls (NC). Patients were diagnosed with 2010 McDonald criteria (Polman *et al.*, 2011) and had to be relapse- and corticosteroid treatment-free for at least 1 month before study entry. NC were recruited among laboratory and hospital workers, had normal neurological examination and no history of neurological disorder.

In MS patients, disability was measured on the Expanded Disability Status Scale (EDSS) (Kurtzke, 1983) whereas cognition was assessed, by a trained and blinded neuropsychologist, using the Brief Repeatable Battery (BRB) (Rao, 1990). BRB incorporates tests of verbal memory acquisition and delayed recall (Selective Reminding Test [SRT]: Long-Term Storage [LTS], Consistent Long-Term Retrieval [CLTR] and Delayed [D]), visual memory acquisition and delayed recall (10/36 Spatial Recall Test [SPART]), attention, concentration and information processing speed (Paced Auditory Serial Addition Test [PASAT]; Symbol Digit Modalities Test [SDMT]) and verbal fluency on semantic stimulus (Word List Generation [WLG]). BRB test failure was defined as score <2 standard deviations from the Italian normative values (Amato *et al.*, 2006) and cognitive impairment was defined as a failure of ≥2 BRB tests.

The cognitive impairment index (CII) score was calculated for each MS patient (Camp *et al.*, 1999; Calabrese *et al.*, 2009). Briefly, the patient was given a grade of 0 if he/she scored at or above the

mean score of the normative value (Amato *et al.*, 2006). Grade 1 was assigned if the patient scored below the control participants' mean score but ≥ 1 standard deviation (SD) below that mean normative value. Grade 2 was assigned if the patient achieved a score > 1 SD but ≤2 SDs below the mean normative value. Finally, grade 3 was assigned if the patient scored > 2 SDs below the mean normative value. These grades were summed across all variables to give one overall measure of cognitive impairment for each patient (Camp *et al.*, 1999; Calabrese *et al.*, 2009). The higher the CII score, the more severe is the cognitive impairment.

The study protocol received approval from the Ethics Committee of Azienda Ospedaliera Universitaria Senese. Informed written consent was obtained from all participants before study entry in accordance with Declaration of Helsinki.

MRI data acquisition

MRI data were acquired before (36 MS patients and 28 NC) and after (64 MS patients and 15 NC) scanner software upgrade using the same imaging protocol, with an 8-channel head coil on a 3 Tesla scanner (Philips Medical Systems, Best, The Netherlands) located at Meyer University Hospital, Florence. A sagittal survey image was used to identify anterior and posterior commissures. Sequences were acquired in the axial plane parallel to the bicommissural line. A dual-echo, turbo spin-echo sequence (repetition time [TR]/echo time [TE]1/TE2= 4000/10/100 ms, voxel size= 1×1×3 mm) yielded proton density (PD) and T2-weighted (T2-W) images. DTI data were an echo-planar imaging (EPI) sequence (TR= 7036 ms; TE= 196 ms; voxel size 2.5 mm3) with 32 diffusion directions and b-value= 900 s/mm2. The resting functional MRI data were 200 volumes of EPI sequence with TR= 3000 ms, TE= 35 ms, voxel size= 1.87 × 1.87 × 4 mm. A high-

resolution (3D) T1-weighted image (T1-W, TR= 10 ms, TE= 4 ms, voxel size= 1 mm^3) was also acquired for image registration, anatomical mapping and analysis of GM images.

MRI data analysis

It was performed at the Quantitative Neuroimaging Laboratory (QNL) of the University of Siena. All images were visually assessed to rule out artifacts or incidental findings.

WM lesions

MS lesions were outlined on PD images by an experienced rater, blinded to patient identity, with a semiautomated segmentation technique based on user-supervised local thresholding (Jim 6.0, Xinapse System, Leicester, UK), which allowed compute global lesion volume (LV).

Regional LV was grouped in anatomically meaningful areas, such as projection, association, commissural, subcortical and brainstem/cerebellar WM (Table 1), in line with previous studies (Hua *et al.*, 2008; Habes *et al.*, 2018). In brief, regional LV was computed using the WM parcellation map (WMPM) of a John Hopkins University (JHU) standard-space atlas (Eve Atlas, www.mristudio.org). First, for each patient LV was calculated in each WM region (label) of the atlas by masking WMPM with the corresponding lesion mask (Oishi *et al.*, 2009). Then, WM regions were divided into 5 groups, such as projection, association, commissural, subcortical and brainstem/cerebellar WM, in line with previous studies (Hua *et al.*, 2008; Habes *et al.*, 2018), and for each anatomically meaningful area, LV was computed by summing the values from all corresponding WM regions (Table 1).

Lesion probability map (LPM) was created through various steps. Briefly, binarized lesion mask of each patient was registered onto MNI152 standard brain through tools of FSL (FMRIB Software Library, http://www.fmrib.ox.ac.uk/fsl) using linear registration (FLIRT [FMRIB Linear Image Registration Too]) (Jenkinson and Smith, 2001) followed by nonlinear registration (FNIRT [FMRIB Non-linear Image Registration Tool]) (Andersson *et al.*, 2007). Two experienced raters (JZ and AG) independently checked all lesion masks registered onto standard brain and an agreement was found in all cases. Finally, LPM was generated first merging and then averaging all lesion masks previously registered onto standard brain.

Table 1. Regions of the WM groups used for the calculation of regional LV

White matter group	*Regions*
Projection WM	Cerebral peduncle, internal capsule (anterior and posterior limbs, retrolenticular part), posterior thalamic radiation, corona radiata (anterior, superior and posterior), sagittal stratum
Association WM	Superior longitudinal fascicle, superior fronto-occipital fascicle, inferior fronto-occipital fascicle, external capsule, uncinate fascicle, cingulum, fornix, stria terminalis
Commissural WM	Corpus callosum (genu, body, splenium), tapetum
Subcortical WM	Superior parietal, frontal (superior, middle, inferior), precentral, postcentral, angular, pre-cuneus, cuneus, lingual, fusiform, occipital (superior, inferior, middle), temporal (superior, inferior, middle), supramarginal, fronto-orbital (lateral, middle), rectus
Brainstem/Cerebellar WM	Corticospinal tract, cerebellar peduncle (superior, inferior, middle), medial lemniscus, pontine crossing tract, cerebellar white matter

See text for abbreviations

Preprocessing of GM, WM and resting FMRI images

It was performed with FSL (FMRIB Software Library, www.fmrib.ox.ac.uk/fsl).

We used, for GM images, the FSL-VBM (voxel-based morphometry) pipeline and, for DTI data, FDT (FMRIB Diffusion Toolbox) to obtain skeletonized-FA images. In addition, MELODIC (multivariate exploratory linear optimized decomposition into IC) was run on resting FMRI data, followed by dual regression and allowed obtain 13 ICs showing high spatial correlation with resting state networks (RSNs) of the literature ("templates").

GM preprocessing

FSL-voxel based morphometry (VBM, https://fsl.fmrib.ox.ac.uk/fsl/fslwiki/FSLVBM) was performed on T1-W images after "filling" hypointense lesions with intensities of the surrounding normal-appearing WM, in order to improve registration and segmentation and thus the resultant volumetric assessment (Battaglini *et al.*, 2012). Briefly, T1-W images were brain-extracted, GM-segmented, and registered onto the MNI152 standard brain using FNIRT nonlinear registration. Then, all native GM images were nonlinearly registered onto a symmetric study-specific GM template, and smoothed with a Gaussian smoothing kernel of 4 mm sigma, corresponding to 9.4 mm full width at half maximum FWHM.

WM preprocessing

DTI data were preprocessed through the FSL program *Eddy*, which corrects for eddy current-induced distortions, subject movement and signal dropout (Andersson and Sotiropoulos, 2016).

Then, we used FDT (FMRIB Diffusion Toolbox) to obtain fractional anisotropy (FA) images by fitting a diffusion tensor model at each voxel. All subjects' FA images were first registered onto a standard-space image (FMRIB58_FA) using FNIRT and then projected onto the mean WM "skeleton" (thresholded at FA> 0.2), resulting in a skeletonized-FA image for each subject.

Resting FMRI preprocessing

The first 5 volumes were removed to allow signal stability, followed by realignment of the remaining volumes to the middle volume (head motion correction), grand mean scaling and spatial smoothing with a 6 mm FWHM Gaussian kernel. ICA-AROMA (independent component analysis-based automatic removal of motion artifacts) was then applied to minimize motion-related artifacts (Pruim *et al.*, 2015). Signals of WM and CSF were regressed out to eliminate the residual structured noise, and high-pass temporal filtering (cut-off frequency= 100 s) was applied. Then, images were normalized onto MNI152 standard brain using FNIRT. Group ICA using MELODIC (multivariate exploratory linear optimized decomposition into independent components [ICs]) was conducted on concatenated normalized images, which were decomposed into 25 ICs (Alfaro-Almagro *et al.*, 2018). Spatial correlation between the 25 ICs and the canonical resting state networks (RSNs) of the literature ("templates") (Smith *et al.*, 2009; Yeo *et al.*, 2011) was estimated using the "fslcc" tool. For further analyses, we considered 12 ICs showing high spatial correspondence (i.e, r≥ 0.4) (Wu *et al.*, 2019) with the RSN templates and also 1 subcortical IC, all obtained with the dual-regression approach (Nickerson *et al.*, 2017).

Data harmonization, spatial down-sampling and normalization

The three MRI modalities were corrected for the effect of scanner software version using the ComBat harmonization approach (Fortin *et al.*, 2017, 2018; Yu *et al.*, 2018). Spatial down-sampling was applied for computational reasons (Groves *et al.*, 2012). In particular, images were down-sampled to a resolution of 4 mm isotropic for VBM and RSNs and of 2 mm isotropic for the skeletonized FA. The three modalities were Z-normalized to ensure the same intensity range and equal contribution to the subsequent fusion analysis (Liang *et al.*, 2019; Liu *et al.*, 2019).

Linked independent component analysis

FMRIB linked ICA (FLICA), also part of FSL, is an extension of Bayesian ICA and allows fusion of multimodal MRI data into a single model, in order to obtain ICs of inter-subject variability (Groves *et al.*, 2011, Llera *et al.*, 2019*a*). In our study, single images of the three MRI modalities (i.e., VBM, skeletonized FA and RSNs) were first concatenated and then decomposed, after 3000 iterations, into 20 ICs (i.e., <25% of the sample size), following the original pipeline (Groves *et al.*, 2011). Each IC consists of spatial maps of all MRI modalities, which are linked together by a single shared subject IC loading coefficient (LC) across modalities, representing the contribution of that subject to the IC. LC of each subject defines the individual relative contribution to the observed spatial pattern. For instance, if a voxel in a modality spatial map has a positive z value, then a lower positive LC in a MS patient than a NC means lower values for that modality (i.e., lower GM density, FA value and FC) and vice versa (Alnæs *et al.*, 2018, Llera *et al.*, 2019*b*). Furthermore, linked ICA also allowed automatic estimation of the contribution of each modality to IC variance.

Statistics

Differences between MS and NC across the three MRI modalities were assessed, using the subject's LC of each IC, in the general linear model framework, with unpaired t-tests, age- and sex-adjusted. Threshold was set at $p<0.05$, False Discovery Rate (FDR)-corrected for multiple comparisons (Winkler *et al.*, 2016). For significant RSNs, the overall trend (i.e., increased or decreased FC) was represented by the mean Z-score within the corresponding thresholded (Z>3) spatial map (Yu *et al.*, 2019).

After identifying the different between-group IC, Spearman coefficient was used to compute in MS group correlation of LC with clinical variables (EDSS and cognition scores) and LV measures (global, log-transformed; regional, Z-transformed).

Furthermore, in order to test the potential effect of global LV, this was used as a covariate in both comparison of linked IC between MS and NC and correlation with clinical measures in the MS group. The correlation coefficients of LC from linked IC and of global LV with clinical measures were compared using Fisher r-to-z transformation (Diedenhofen and Musch, 2015).

All analyses were performed with R software (https://www.r-project.org/).

To test similarity of spatial maps obtained between fusion analysis performed with and without RSNs (i.e., structural-functional vs structural fusion) we computed voxelwise spatial cross-correlation (Douaud et al., 2014; Smith et al., 2019) for each modality of significantly linked IC. In addition, visual inspection of spatial maps was also performed.

Results

Clinical, demographic and LV characteristics

Compared to NC, MS patients were similar for sex (p=0.927) and marginally older (p=0.05). Data are summarized in Table 2.

Table 2. Clinical, demographic and LV characteristics of the study groups

	RR MS patients	*NC*	*p-value*
Age (mean±SD, y)	39.7 ± 10.5	35.8 ± 10.5	0.05[a]
Sex (male/female no.)	31/69	13/30	0.927[b]
Disease duration (mean±SD, y)	9.4 ± 6.9	-	-
EDSS (median [range])	1.5 (0-6.5)	-	-
Cognitive impairment (yes/no) [%]	30/70 [30%]	-	-
LV (median [range], cm^3)	3.50 (0.10-71.90)	-	-
Projection (median [range], cm^3)	3.4 (0.22-32.39)	-	-
Association (median [range], cm^3)	0.33 (0-9.28)	-	-
Commissural (median [range], cm^3)	1.19 (0.06-9.35)	-	-
Subcortical (median [range], cm^3)	1.74 (0.09-33.25)	-	-
Brainstem/cerebellar (median [range], cm^3)	0.09 (0-1.51)	-	-

Abbreviations
MS: multiple sclerosis; NC: normal control; SD: standard deviation; EDSS: Expanded Disability Status Scale; LV: lesion volume.
[a]Two-sample t-test
[b]Chi-squared test
See text for abbreviations

Linked structural (GM density, skeletonized WM FA) and functional (RSNs) alterations

Out of 20 structural and functional linked ICs, only one (IC6) showed significant difference between MS and NC (p=0.004, FDR-corrected). After correcting for global LV, the difference was retained (p=0.030, FDR-corrected). Modality contribution to the variance of such IC was 44% for VBM, 38% for skeletonized FA and 18% for all RSNs.

Linked GM atrophy

MS patients showed linked GM atrophy compared to NC in cortical GM (precentral and postcentral gyrus), deep GM (caudate, putamen and thalamus) and cerebellar cortex (Fig. 1A, Table 3).

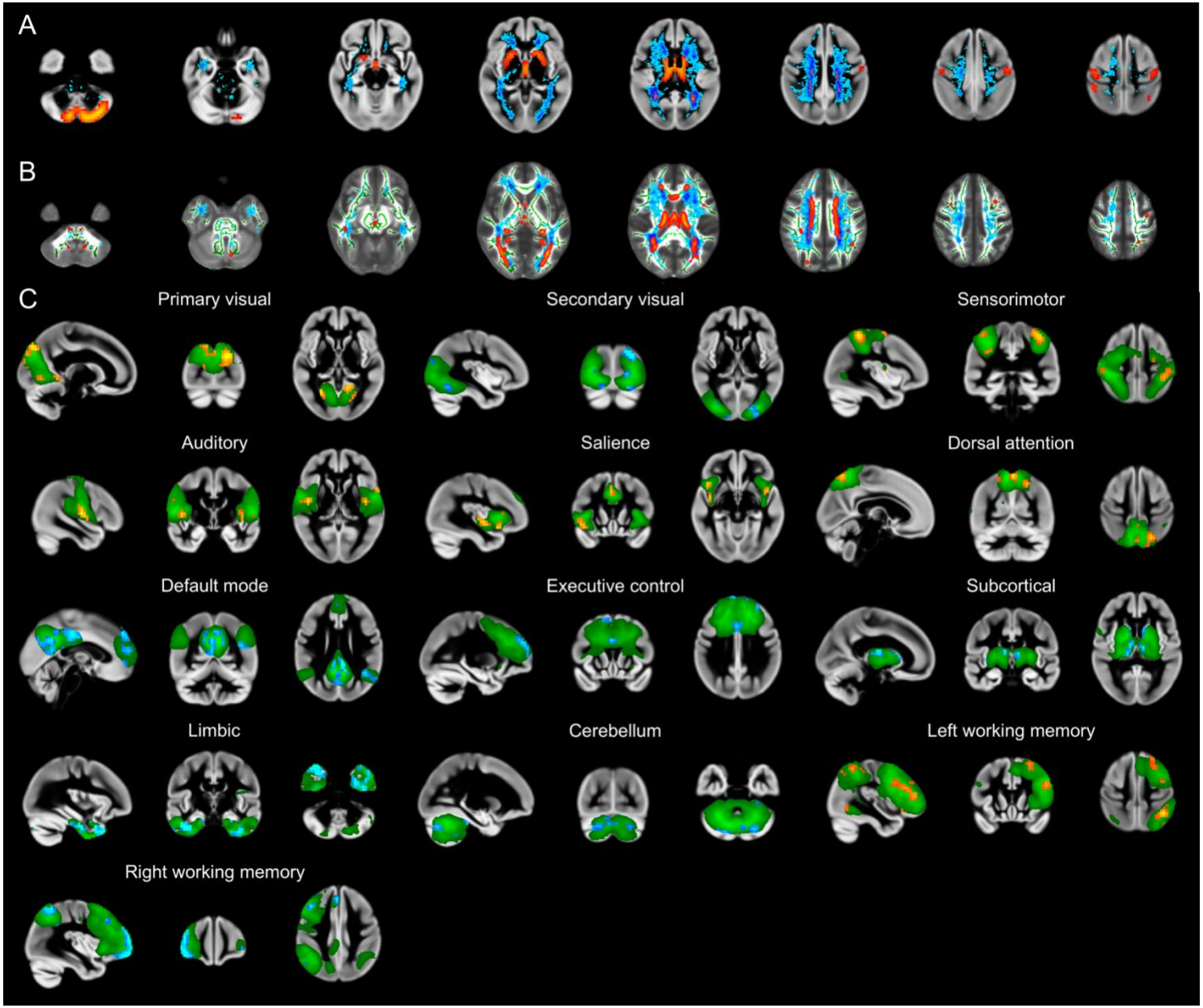
A
B
C
Primary visual
Secondary visual
Sensorimotor
Auditory
Salience
Dorsal attention
Default mode
Executive control
Subcortical
Limbic
Cerebellum
Left working memory
Right working memory

Figure 1. Linked GM atrophy (A), WM microstructural damage (i.e., decreased FA, B) and FC anomalies in RSNs (C) in MS patients compared to NC. Red-yellow indicates GM atrophy (A), WM microstructural damage (B) and decreased FC in RRMS. Blu-light blu indicates increased FC in RRMS (C). Green represents brain networks (derived from MELODIC, C). Lesion probability map (in light-blue to red, range: 1-31%) is also shown (A-B) to assess the spatial relationship of GM atrophy and WM microstructural damage with lesions. Background images are the UK Biobank GM template for GM density and RSNs and FMRIB58_FA standard space for WM microstructure, respectively, shown in radiological convention. See text for abbreviations; a.u.: arbitrary unit.

Table 3. Regions of linked GM atrophy and WM microstructural damage (p=0.004, FDR-corrected) within significantly linked IC (IC6) in MS patients compared to NC

	Brain region (local maxima)	*Side*	*MNI (x, y, z)*	*Z-value*
Linked GM atrophy				
Cortical GM	Precentral Gyrus	L	-36, -24, 58	3.0
	Postcentral Gyrus	R	44, -20, 58	3.1
	Postcentral Gyrus	L	-32, -28, 62	3.2
	Precentral Gyrus	R	24, -28, 66	3.2
Deep GM	Putamen	L	-16, 12, -6	3.6
	Putamen	R	20, 12, -6	3.6
	Caudate	L	-10, 8, 14	3.5
	Caudate	R	12, 8, 14	3.1
	Thalamus	L	-8, -12, 18	3.6
	Thalamus	R	8, -8, 18	3.6

Cerebellar cortex		R	40, -60, -50	2.3
		L	-32, -76, -46	4.4
Linked WM microstructural damage				
Projection WM	Anterior thalamic radiation	R	1, -19, -9	7.7
	Posterior thalamic radiation/optic radiation	L	-31, -63, -1	6.4
	Posterior thalamic radiation/optic radiation	R	33, -65, 11	5.5
	Anterior thalamic radiation	L	-15, -23, 17	13.7
Association WM	Superior longitudinal fascicle	L	-41, -57, 7	3.0
	Inferior fronto-occipital fascicle	L	-33, 31, 11	3.8
	Inferior fronto-occipital fascicle	R	31, -49,17	5.8
	Superior longitudinal fascicle	R	33, -35, 35	3.2

Commissural WM	Cingulum	L	-23, -49, 1	5.3
	Cingulum	R	25, -47, 1	5.9
	Body of corpus callosum	R	19, 15, 29	6.5
	Body of corpus callosum	L	-15, 9, 31	6.3
Brainstem/cerebellar WM	Middle cerebellar peduncle	R	13, -25, -37	4.3
	Corticospinal tract	L	-1, -21, -35	2.7
	Corticospinal tract	R	13, -25, 67	4.3

Brain regions were ordered by increasing coordinates on the z-axis

Abbreviations
FDR: false discovery rate; L: left; R: right; M: middle; GM: grey matter; WM: white matter; IC: independent component; MS: multiple sclerosis; NC: normal control.

Linked WM microstructural damage

Linked lower FA in MS than NC was found in projection WM (anterior and posterior thalamic radiation [ATR and PTR]), association WM (superior longitudinal fascicle [SLF], inferior fronto-occipital fascicle [IFOF]), commissural WM (cingulum [Cg], body of the corpus callosum [CC]) and brainstem/cerebellar WM (corticospinal tract [CST], middle cerebellar peduncle [MCP]) (Fig. 1B, Table 3).

Linked FC alterations within RSNs

All RSNs were altered in MS patients compared to NC. In particular, we found both linked decreased FC (primary visual [VN], sensorimotor [SMN], auditory/language [AUD/LAN], salience [SN], dorsal attention [DAN], fronto-parietal left working memory networks [WMN]) and linked increased FC (secondary VN, default mode [DMN], executive control [ECN], fronto-parietal right WMN, subcortical [SCN], limbic [LN] and cerebellum [CbN] networks) (Fig. 1C).

LC from linked IC was significantly lower in cognitively impaired (CI) than in cognitively preserved (CP) MS (p=0.004, Fig. 2).

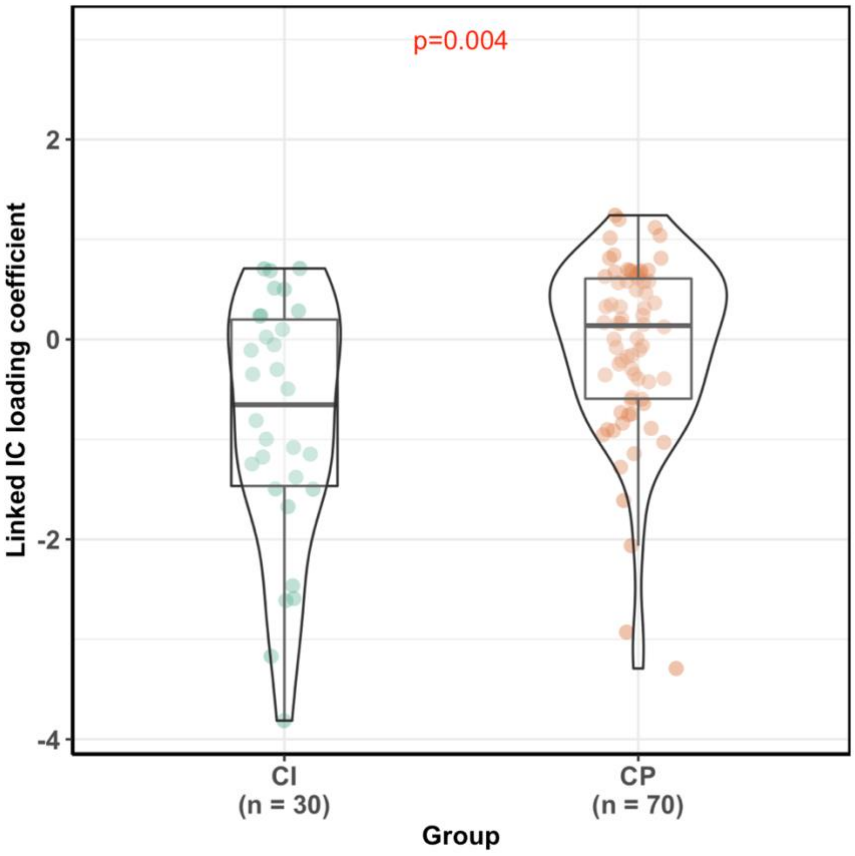

Figure 2. Cognitively impaired (CI) MS showed significantly lower loading coefficient (LC) of linked independent component (IC) than cognitively preserved (CP) MS.

Correlation of linked structural and functional alterations with clinical and LV measures

LC from significant structural and functional linked IC (IC6) showed in MS group correlation with EDSS (r=-0.35, p<0.001), Selective Reminding Tests (SRT, r=0.39, p<0.001 for Long-Term Storage [LTS]; r=0.44, p<0.001 for Consistent Long-Term Retrieval [CLTR]; r=0.40, p<0.001 for Delayed [D]), Spatial Recall Test (SPART) (r=0.30, p=0.003), Symbol Digit Modalities Test (SDMT) (r=0.35, p<0.001) and CII (r=-0.39, p<0.001) (Table 4).

On the other hand, global LV showed, with respect to LC, weaker (p<0.001 for all) correlation with EDSS (r=0.30, p=0.002), SRT-CLTR (r=-0.38, p<0.001), SRT-D (r=-0.33, p<0.001), CII (r=0.36, p<0.001), SDMT (r=-0.34, p<0.001) and stronger correlation (p<0.001) with SRT-LTS (r=-0.44, p<0.001) (Table 4).

Table 4. Significant correlation of LC from the significant between-group (MS vs NC) structural and functional linked IC and of global LV with clinical measures in the MS group

	EDSS	*SRT-LTS*	*SRT-CLTR*	*SRT-D*	*SDMT*	*CII*
LC of IC6	-0.35	0.39	0.44	0.40	0.35	-0.39
	(p<0.001)	(p<0.001)	(p<0.001)	(p<0.001)	(p<0.001)	(p<0.001)
LV	0.30	-0.44	-0.38	-0.33	-0.34	0.36
	(p=0.002)	(p<0.001)	(p<0.001)	(p<0.001)	(p<0.001)	(p<0.001)

Fisher transformation	r-to-z	z=-3.64 (p<0.001)	z=4.76 (p<0.001)	z=4.70 (p<0.001)	z=4.13 (p<0.001)	z=3.88 (p<0.001)	z=-4.25 (p<0.001)

Abbreviations
LC: loading coefficient; IC: independent component; LV: lesion volume; MS: multiple sclerosis; NC: normal control; EDSS: Expanded Disability Status Scale; SRT-LTS: Selective Reminding Tests for Long-Term Storage; SRT-CLTR: Selective Reminding Tests for Consistent Long-Term Retrieval; SRT-D: Selective Reminding Tests for Delayed; SDMT: Symbol Digit Modalities Test: CII: Cognitive Impairment Index.

LC from the significantly linked IC (IC6) showed correlation with global LV (r=-0.67, p<0.001) and with regional LV (r values from -0.24 to -0.65, p<0.05) (Table 5). The anatomical relationship of GM atrophy and WM microstructural damage within significantly linked IC with LPM is shown in Fig. 1A-B.

Table 5. Correlation of LC from the significant between-group (MS vs NC) structural and functional linked IC (IC6) with LV measures (global and regional) in the MS group

LV	*Global*	*Projection*	*Association*	*Commissural*	*Subcortical*	*Brainstem/Cerebellar*
LC of IC6	-0.67 (p<0.001)	-0.65 (p<0.001)	-0.59 (p<0.001)	-0.60 (p<0.001)	-0.63 (p<0.001)	-0.24 (p<0.001)

Abbreviations
LC: loading coefficient; IC: independent component; MS: multiple sclerosis; NC: normal control: LV: lesion volume

Linked structural (GM density, skeletonized WM FA) alterations

Out of 20 structural linked ICs, only one (IC1) showed significant difference between MS and NC (p=0.002, FDR-corrected). After correcting for global LV, the difference was retained (p=0.037, FDR-corrected). Modality contribution to the variance of IC1 was 57% for VBM and 43% for

skeletonized WM FA. These spatial maps of VBM and skeletonized FA showed spatial similarity to those (r=0.99 for both) of linked structural and functional alterations.

LC of IC1 was lower in CI than in CP MS (p=0.002).

Similarly to the main fusion analysis (i.e., linked structural and functional IC), correlation strength of LC with clinical and LV measures were largely unchanged (Table 6, Table 7) and LC showed a significantly closer correlation than global LV with clinical measures (p<0.001), expect for SRT-LTS (p<0.001) (Table 6).

Table 6. Correlation of LC from the significant between-group (MS vs NC) structural (GM density, skeletonized WM FA) linked IC and of LV with clinical measures in the MS group

	EDSS	*SRT-LTS*	*SRT-CLTR*	*SRT-D*	*SDMT*	*CII*
LC of IC1	-0.38	0.40	0.44	0.40	0.37	-0.40
	(p<0.001)	(p<0.001)	(p<0.001)	(p<0.001)	(p<0.001)	(p<0.001)
LV	0.30	-0.44	-0.38	-0.33	-0.34	0.36
	(p=0.002)	(p<0.001)	(p<0.001)	(p<0.001)	(p<0.001)	(p<0.001)
Fisher r-to-z transformation	z=-3.83 (p<0.001)	z=4.84 (p<0.001)	z=4.71 (p<0.001)	z=4.14 (p<0.001)	z=4.01 (p<0.001)	z=-4.32 (p<0.001)

Abbreviations
LC: loading coefficient; IC: independent component; LV: lesion volume; MS: multiple sclerosis; NC: normal control; EDSS: Expanded Disability Status Scale; SRT-LTS: Selective Reminding Tests for Long-Term Storage; SRT-CLTR: Selective Reminding Tests for Consistent Long-Term Retrieval; SRT-D: Selective Reminding Tests for Delayed; SDMT: Symbol Digit Modalities Test: CII: Cognitive Impairment Index.

Table 7. Correlation of LC from the significant between-group (MS vs NC) structural (GM density, skeletonized WM FA) linked IC with LV measures (global and regional) in the MS group

LV	*Global*	*Projection*	*Association*	*Commissural*	*Subcortical*	*Brainstem/Cerebellar*
LC of IC1	-0.66 (p<0.001)	-0.66 (p<0.001)	-0.60 (p<0.001)	-0.58 (p<0.001)	-0.64 (p<0.001)	-0.24 (p=0.018)

Abbreviations
LC: loading coefficient; IC: independent component; MS: multiple sclerosis; NC: normal control: LV: lesion volume

Discussion

In this study, we "fused" for the first time in MS structural and functional MRI modalities, in order to directly investigate common pathogenic mechanisms of WM and GM.

Concurrent structural and functional alterations in RRMS

Compared to the other two fused MRI measures (WM microstructural integrity and FC in RSN), atrophy in sensorimotor cortex, deep and cerebellar GM dominated, with 44% contribution, the linked IC showing difference between MS and NC, thus highlighting the main pathogenic relevance of neurodegeneration in key GM regions of MS brain. Skeletonized FA in all WM tract systems revealed a good contribution (38%) to the linked IC variance, suggesting an additional pathogenic role for WM microstructural damage in tracts of all WM systems. FC within RSNs as a whole showed the lowest contribution, in the order of 18%, to the linked IC, probably reflecting complex and widespread short-range FC abnormalities in the MS brain.

Controlling for the effect of global LV did not affect the difference between MS and NC in the linked IC, suggesting that structural and functional co-alterations may be independent of WM lesions, in line with previous unimodal MRI studies (Henry *et al.*, 2009; Filippi and Rocca, 2010; Jehna *et al.*, 2013). Thus, our findings lend support to the idea that in MS structural and functional co-alterations, here directly assessed for the first time, play an important role in the disease pathogenesis, beyond macroscopic WM lesions (Filippi *et al.*, 2019*c*; Koubiyr *et al.*, 2019).

The highest contribution (44%) of GM atrophy to the linked IC variance supports the notion that GM atrophy, a proxy for neurodegeneration, plays a key role to the MS pathogenesis (De Stefano *et al.*, 2014). In previous studies, GM atrophy was found to be greater in patients with CIS who developed MS and in patients with established MS who showed sustained progression of disability than those who were stable (De Stefano *et al.*, 2014). Moreover, GM atrophy over a 4-year period accumulated with disease stage, being 8.1 times greater in patients with RRMS than in NC (Fisher *et al.*, 2008).

Within the significantly linked IC, atrophy mapping on sensorimotor cortex, deep and cerebellar GM is consistent with previous unimodal MRI studies (Bodini *et al.*, 2009*b*; Anderson *et al.*, 2011; Steenwijk *et al.*, 2016; Eshaghi *et al.*, 2018). In pathogenic terms, atrophy in sensorimotor cortex (i.e., precentral and postcentral gyrus) may be due to CSF-mediated factors (Rocca *et al.*, 2017) and/or meningeal inflammatory infiltrates (Zurawski *et al.*, 2017; Machado-Santos *et al.*, 2018) while for cerebellar atrophy an important role for demyelination and meningeal inflammation has been proposed (Parmar *et al.*, 2018). Atrophy in deep GM (i.e., putamen, caudate and thalamus) may be the result of demyelination, inflammation, axonal injury, iron deposition and oxidative stress (Haider *et al.*, 2014). More importantly, the involvement of cerebellum, sensorimotor and

deep GM in the same linked IC of a RRMS group with mild disability, as in our study, suggests the co-variation of different GM regions, beyond the traditional idea that different GM regions are separately involved in different disease stages (Rocca *et al.*, 2017).

Concurrent WM microstructural damage within the significantly linked IC comprised all the WM tract systems such as projection (ATR, PTR), association (SLF, IFOF), commissural (Cg, CC body) and brainstem/cerebellar (CST, MCP). This widespread damage was previously reported in MS, although in various single DTI studies (Enzinger *et al*., 2015). In our study, FA of lesion areas and NAWM co-decreased in the projection (lesional PTR and normal-appearing [NA] ATR), association (lesional IFOF and NA SLF) and commissural (lesional body of CC and NA Cg) WM.

The significantly linked IC also showed widespread concurrent alterations of short-range FC. In particular, this was decreased, at the level of primary sensory RSNs, in primary VN, SMN and AUD/LAN reflecting, respectively, altered function in the visual (Gallo *et al.*, 2012; Tahedl *et al.*, 2018), motor (Tahedl *et al.*, 2018), auditory/language (Maudoux *et al.*, 2012) networks and also increased in the secondary VN, with a plausible adaptive/compensatory meaning (Tahedl *et al.*, 2018).

As for cognition-related RSN, short-range FC was decreased, in line with previous unimodal resting FMRI studies (Rocca *et al.*, 2012; Tahedl *et al.*, 2018), in the SN and DAN, suggesting a possible deficient integration of emotional/sensory stimuli and attention tasks. On the other hand, increased FC was found in the DMN and ECN as possible maladaptation towards cognitive efficiency (Hawellek *et al.*, 2011) and in the SCN, LN and CbN as expression of adaptive/ compensatory mechanisms towards a reduction of, respectively, neural processing (Dogonowski

et al., 2013), memory function (Enzinger *et al.*, 2016), attention-demanding tasks and social cognition (Cocozza *et al.*, 2018). It is worth noting that for fronto-parietal WMN, FC was found to be decreased on the left and increased on the right hemisphere, these homotopic alterations probably reflecting a deficient working memory in MS, as already reported in healthy subjects and psychiatric conditions (Yamashita *et al.*, 2018).

Brain regional alterations in our RRMS group not only showed a link among them but also spatial relationships. In particular, atrophy in sensorimotor cortex was spatially adjacent to decreased FA in association WM tracts (SLF, IFOF), probably due to a suppression of neurotrophic effects of WM on GM from myelin and axonal injury (Han *et al.*, 2017).

Moreover, atrophy in deep GM regions, also found in our significantly linked IC, may be attributed to retrograde and anterograde neurodegeneration of connecting WM tracts such as PTR (Kolasinski *et al.*, 2012; Eshaghi *et al.*, 2018), a type of projection WM, which indeed was found co-damaged in our study.

Though a previous study did not find association between cerebellar atrophy and decreased FA of MCP (Anderson *et al.*, 2011), the linked damage of these two regions in our significantly linked IC suggests the presence of an inter-relationship which may go undetected by unimodal MRI studies (Parmar *et al.*, 2018).

Interestingly, significantly linked IC also showed some high between-modality spatial overlap involving sensorimotor, deep, cerebellum atrophy and corresponding short-range FC which seems to point to the presence of compensatory mechanisms of local FC towards corresponding local GM atrophy (Louapre *et al.*, 2014; Tahedl *et al.*, 2018).

Very recently, it was demonstrated through a multiple linear regression model on a very large population of healthy subjects, a relationship between FC across brain regions and integrity of connecting WM tracts, suggesting that WM microstructure may affect neural circuit activity through conduction speed (Mollink *et al.*, 2019). In line with the above study, we demonstrated that linked microstructure-function relationships do exist and may be altered in a complex neurological condition such as MS.

Caution should be taken when assessing in MS the pathogenic effect of co-occurring structural and functional brain abnormalities. In a recent study, while both cortical and thalamic GM damage induced a global increase in FC, WM damage induced first an increase and then a decrease in FC (Tewarie *et al.*, 2018). When interpreting increased FC values in cross-sectional studies as "compensation", the disease stage and level of tissue damage in GM and/or WM should be considered, in view that a proportion of altered FC may be simply the result of structural damage (Tewarie *et al.*, 2018) and not an adaptive or maladaptive primary process of the GM.

Of note, when only assessing the pathogenic effect of structural MRI modalities on the between-group (MS vs NC) comparison, there was an increased contribution to the linked IC of both regional GM atrophy (from 44% to 57%) and skeletonized WM FA (from 38% to 43%). In our study, both increased and decreased FC co-occur in the significant between-group linked IC. Because these two processes may coexist in the human brain (Bijsterbosch *et al.*, 2019), the net effect of altered FC across RSNs may be balanced in our study, and this may explain the similarity in the clinical correlations of linked structural anomalies with and without functional anomalies, as commented in the next paragraph.

Clinical relevance of concurrent structural and functional alterations in RRMS

Co-occurrence of linked GM atrophy, WM microstructural damage and abnormal short-range FC moderately correlated with higher physical disability, as measured on EDSS. However, results of linked structural MRI modalities only (i.e., VBM and TBSS of FA) provided overall similar correlation strength. This may be in theory explained by the fact that while GM atrophy and WM microstructural damage showed a single directional change due to tissue damage, RSNs showed both increased and decreased FC, probably corresponding to opposite mechanisms, as explained above, indicating that in our RRMS group with mild disability, adaptive and maladaptive FC in RSNs might be balanced.

Previous unimodal GM atrophy studies reported an association between sensorimotor cortex and physical disability (Bodini *et al.*, 2009*a*; Narayana *et al.*, 2012; Steenwijk *et al.*, 2016). Moreover, atrophy in deep GM was recently shown to drive disability worsening in MS (Eshaghi *et al.*, 2018). Finally, cerebellar atrophy was related to progressive disability (Parmar *et al.*, 2018).

As for WM microstructure, all the involved tracts of our linked IC were reported in previous unimodal DTI studies to be associated with physical disability (Welton *et al.*, 2014; Enzinger *et al.*, 2015).

Various previous unimodal MRI studies have reported that cortical and deep GM atrophy, WM microstructural injury and altered FC were separately associated with cognitive impairment (Sumowski et al., 2018). A challenging but essential step would be to integrate multimodal MRI data in order to provide a common pathologic substrate for cognitive impairment (Sumowski *et*

al., 2018). Our current results provide early evidence that linked brain regions of GM atrophy, WM microstructural damage and abnormal short-range FC may be such substrate, thus potentially being a future treatment target in MS (Sumowski *et al.*, 2018). It was recently reported that cognitive deficits in MS may accelerate in parallel with greater structural damage and less efficient FC (Koubiyr *et al.*, 2019). Our result of a lower LC from linked regions of GM atrophy, WM microstructural injury and altered FC in cognitively impaired than preserved MS group is in line with the above hypothesis.

Although cognitive impairment was only present in 30% of our MS group, the significantly linked IC showed moderate correlations with various cognitive domains, in particular with long-term memory retrieval, suggesting that concurrent linked anatomical and functional abnormalities are sensitive to cognitive impairment in RRMS with mild disability.

CII takes into account the global cognitive impairment of each individual patient (Camp *et al.*, 1999). In our study, CII correlated moderately with LC of linked IC, prompting that such multimodal MRI index needs to be tested in future studies on more disabled MS patients not only for specific cognitive domains but also for global cognition, with a possible future translation into clinical practice (Camp *et al.*, 1999; Calabrese *et al.*, 2009).

It was recently reported that singularly assessed deep GM atrophy, reduced widespread WM integrity and increased whole brain FC were the best predictors for impaired information processing in MS (Meijer *et al.*, 2018). However, FC of that study was an overall measure and as such not evaluating the role of single brain networks. By contrast, our study found that FC in each

RSN was either increased or decreased and as such might be more informative for mapping specific brain structures and functions as possible therapeutic targets (Sumowski *et al.*, 2018).

In previous unimodal MRI studies on cognitive impairment, deep GM atrophy was reported to be one of the predictors in RRMS (Eijlers *et al.*, 2018). Cerebellar atrophy was related to cognitive impairment, in particular executive function and working memory (Parmar *et al.*, 2018). In addition, decreased FA in CC, SLF, CST and Cg was associated with cognitive impairment in MS (Enzinger *et al.*, 2015). Finally, the above WM tracts showed more extensive FA reduction in cognitively impaired than in cognitively preserved MS patients (Hulst *et al.*, 2013).

Significantly linked IC moderately correlated with global and regional LV and this confirms the key role of MS lesions for widespread brain alterations (Filippi *et al.*, 2019*b*).

We found that linked IC correlated significantly better than global LV with almost all the clinical measures, pointing out the higher clinical relevance of shared structural and functional alterations compared to the WM macroscopic damage. An interesting exception was that global LV showed slightly higher correlation with long-term memory than LC of linked IC. A possible explanation is that structural macroscopic damage such as WM lesions in MS may be more important than shared structural and functional changes to specific impaired cognitive domain, as is the case of long-term memory (Llera *et al.*, 2019*b*).

Though the current results indicate that shared structural and functional alterations show some relevance for MS clinical status, there is more to be done to complete the complex MS pathological picture. Recently, it was shown that higher dynamic FC of hippocampal itself, changing over time, independently of its atrophy, was related to worse verbal and visuospatial learning and memory

performance (Geest *et al.*, 2018). This reminds us that for disease pathogenesis, different MRI modalities not only show shared pathogenic mechanisms, but also have distinct trajectories over time (Lahat *et al.*, 2015; Akhonda *et al.*, 2019). Starting from this, combining the shared structural and functional alterations and the distinctive structural/functional changes over time would be helpful in future for stratification of MS pathogenic mechanisms.

Strengths and limitations

Linked ICA seems to ideally overcome some limitations of graph theory-based multimodal MRI analysis, including predefined "nodes" for each modality, atlas-based parcellation, arbitrarily thresholded correlation matrix, high degree of abstraction of network matrix, and thus a combination of unimodal results (Filippi *et al.*, 2017, 2018*b*) which may bias interpretation and ignore multimodal cross-information (Smith, 2012; Calhoun and Sui, 2016). Moreover, linked ICA turns out be more straightforward to interpret compared to canonical correlation analysis (CCA), whose correlation coefficients may not be sufficiently distinct (Calhoun and Sui, 2016, Llera *et al.*, 2019*a*). Finally, linked ICA allows a more individualized assessment of each MRI modality compared to joint ICA, a different type of fusion method (Llera *et al.*, 2019*a*; Wu *et al.*, 2019).

However, there are some limitations to our study. First, only RRMS patients were included and thus future studies should also assess linked pathogenic mechanisms in other MS phenotypes. Second, longitudinal studies are warranted in order to investigate the trajectories of the linked WM

and GM abnormalities over time. Third, WM lesions distribution should be incorporated into the fusion model in future, in order to directly assess the contribution of WM lesions .

In conclusion, by using a multivariate method on combined multimodal MRI data, we showed for the first time that linked structural and functional alterations exist in RRMS patients. These multidimensional brain underpinnings of MS may provide novel clues about disease mechanisms that may ultimately lead to novel treatments in MS patients.

Summary

Background: There is still need to bridge the gap in linking structural and functional anomalies in the multiple sclerosis (MS) brain, in order to better clarify its complex pathogenic scenario. Multimodal MRI data-driven fusion, by modeling shared contribution across combined modalities, is able to identify co-occurring alterations across brain.

Objective: To uncover in MS the hidden direct relationships between brain structural damage and functional alterations, and the shared pathophysiology across different MRI modalities

Methods: We included 100 relapsing-remitting MS patients (age: 39.7±10.5 years, duration: 9.4±6.9 years, median EDSS: 1.5, cognitive impairment: 30%) and 43 normal controls (NC, age: 35.8±10.5 years). FMRIB linked independent component (IC) analysis, a type of fusion approach, was used to simultaneously assess grey matter (GM) density, white matter (WM) microstructure and functional connectivity (FC) within brain networks.

Results: One linked structural-functional IC, out of 20, showed significant (p=0.004, corrected) between-group difference and included sensorimotor, subcortical, cerebellar atrophy (44% contribution), diffuse decreased fractional anisotropy in WM (projection, association, commissural and brainstem/cerebellar) (38% contrivution) and altered short-range FC in all resting state nnetworks (18%). Some of these linked alterations were also spatially adjacent or overlapping with each other. These linked alterations showed a moderate relationship with physical disability (r=-0.35, p<0.001) and impairment of specific cognitive domains, especially long-term memory (r=0.44, p<0.001).

Conclusion: Our study uncovered for the first time in MS the direct and shared structure-function pathogenic mechanisms.

7 Conclusions of the two studies presented

1. Non-random and distinct anatomical patterns of GM atrophy and WM microstructural damage seem to occur at group level in RRMS patients with mild disability, and to be differently inter-related.

2. By fusing in MS structural and functional MRI modalities, we characterized linked structural and functional alterations that are able to differentiate MS patients and NC. By showing correlations between LC from linked IC and clinical measures, we have characterized a single pathogenic and clinically relevant MRI index.

8 References

Absinta M, Sati P, Schindler M, Leibovitch EC, Ohayon J, Wu T, et al. Persistent 7-tesla phase rim predicts poor outcome in new multiple sclerosis patient lesions. J Clin Invest 2016; 126: 2597–2609.

Akhonda MABS, Long Q, Bhinge S, Calhoun VD, Adali T. Disjoint Subspaces for Common and Distinct Component Analysis: Application to Task FMRI Data. In: 2019 53rd Annual Conference on Information Sciences and Systems (CISS). 2019. p. 1–6

Alexander AL, Lee JE, Lazar M, Field AS. Diffusion tensor imaging of the brain. Neurotherapeutics 2007; 4: 316–329.

Alfaro-Almagro F, Jenkinson M, Bangerter NK, Andersson JLR, Griffanti L, Douaud G, et al. Image processing and Quality Control for the first 10,000 brain imaging datasets from UK Biobank. NeuroImage 2018; 166: 400–424.

Alnæs D, Kaufmann T, Doan NT, Córdova-Palomera A, Wang Y, Bettella F, et al. Association of Heritable Cognitive Ability and Psychopathology With White Matter Properties in Children and Adolescents. JAMA Psychiatry 2018; 75: 287–295.

Amato MP, Portaccio E, Goretti B, Zipoli V, Ricchiuti L, Caro MFD, et al. The Rao's Brief Repeatable Battery and Stroop test: Normative values with age, education and gender corrections in an Italian population. Mult Scler 2006; 12: 787–793.

Amato MP, Portaccio E, Stromillo ML, Goretti B, Zipoli V, Siracusa G, et al. Cognitive assessment and quantitative magnetic resonance metrics can help to identify benign multiple sclerosis. Neurology 2008; 71: 632–638.

Anderson V, Wheeler-Kingshott C, Abdel-Aziz K, Miller D, Toosy A, Thompson A, et al. A comprehensive assessment of cerebellar damage in multiple sclerosis using diffusion tractography and volumetric analysis. Mult Scler 2011; 17: 1079–1087.

Andersson JL, Jenkinson M, Smith S, others. Non-linear registration, aka spatial normalisation [Internet]. FMRIB technical report TR07JA2 2007[cited 2016 Jul 7] Available from: https://www.fmrib.ox.ac.uk/analysis/techrep/tr07ja2/tr07ja2.pdf

Andersson JLR, Sotiropoulos SN. An integrated approach to correction for off-resonance effects and subject movement in diffusion MR imaging. Neuroimage 2016; 125: 1063–1078.

Battaglia M, Kobelt G, Ponzio M, Berg J, Capsa D, Dalén J, et al. New insights into the burden and costs of multiple sclerosis in Europe: Results for Italy. Mult Scler 2017; 23: 104–116.

Battaglia MA, Bezzini D. Estimated prevalence of multiple sclerosis in Italy in 2015. Neurol Sci 2017; 38: 473–479.

Battaglini M, Jenkinson M, De Stefano N. Evaluating and reducing the impact of white matter lesions on brain volume measurements. Hum Brain Mapp 2012; 33: 2062–2071.

Bergsland N, Horakova D, Dwyer MG, Uher T, Vaneckova M, Tyblova M, et al. Gray matter atrophy patterns in multiple sclerosis: A 10-year source-based morphometry study. NeuroImage: Clinical 2018; 17: 444–451.

Bijsterbosch JD, Beckmann CF, Woolrich MW, Smith SM, Harrison SJ. The relationship between spatial configuration and functional connectivity of brain regions revisited. Elife 2019; 8

Bjartmar C, Wujek JR, Trapp BD. Axonal loss in the pathology of MS: Consequences for understanding the progressive phase of the disease. J Neurol Sci 2003; 206: 165–171.

Bodini B, Battaglini M, De Stefano N, Khaleeli Z, Barkhof F, Chard D, et al. T2 lesion location really matters: A 10 year follow-up study in primary progressive multiple sclerosis. J Neurol Neurosurg Psychiatry 2011; 82: 72–77.

Bodini B, Cercignani M, Khaleeli Z, Miller DH, Ron M, Penny S, et al. Corpus callosum damage predicts disability progression and cognitive dysfunction in primary-progressive MS after five years. Hum Brain Mapp 2013; 34: 1163–1172.

Bodini B, Chard D, Altmann DR, Tozer D, Miller DH, Thompson AJ, et al. White and gray matter damage in primary progressive MS: The chicken or the egg? Neurology 2016; 86: 170–176.

Bodini B, Khaleeli Z, Cercignani M, Miller DH, Thompson AJ, Ciccarelli O. Exploring the relationship between white matter and gray matter damage in early primary progressive multiple sclerosis: An in vivo study with TBSS and VBM. Human Brain Mapping 2009; 30: 2852–2861.

Bodini B, Khaleeli Z, Cercignani M, Miller DH, Thompson AJ, Ciccarelli O. Exploring the relationship between white matter and gray matter damage in early primary progressive multiple sclerosis: An in vivo study with TBSS and VBM. Hum Brain Mapp 2009; 30: 2852–2861.

Bonavita S, Gallo A, Sacco R, Corte MD, Bisecco A, Docimo R, et al. Distributed changes in default-mode resting-state connectivity in multiple sclerosis. Mult Scler 2011; 17: 411–422.

Browne P, Chandraratna D, Angood C, Tremlett H, Baker C, Taylor BV, et al. Atlas of Multiple Sclerosis 2013: A growing global problem with widespread inequity. Neurology 2014; 83: 1022–1024.

Brownlee WJ, Hardy TA, Fazekas F, Miller DH. Diagnosis of multiple sclerosis: Progress and challenges. The Lancet 2017; 389: 1336–1346.

Calabrese M, Agosta F, Rinaldi F, Mattisi I, Grossi P, Favaretto A, et al. Cortical Lesions and Atrophy Associated With Cognitive Impairment in Relapsing-Remitting Multiple Sclerosis. Arch Neurol 2009; 66: 1144–1150.

Calhoun VD, Sui J. Multimodal fusion of brain imaging data: A key to finding the missing link(s) in complex mental illness. Biol Psychiatry Cogn Neurosci Neuroimaging 2016; 1: 230–244.

Camp SJ, Stevenson VL, Thompson AJ, Miller DH, Borras C, Auriacombe S, et al. Cognitive function in primary progressive and transitional progressive multiple sclerosisA controlled study with MRI correlates. Brain 1999; 122: 1341–1348.

Ceccarelli A, Rocca MA, Pagani E, Colombo B, Martinelli V, Comi G, et al. A voxel-based morphometry study of grey matter loss in MS patients with different clinical phenotypes. Neuroimage 2008; 42: 315–322.

Cocozza S, Pontillo G, Russo C, Russo CV, Costabile T, Pepe A, et al. Cerebellum and cognition in progressive MS patients: Functional changes beyond atrophy? J Neurol 2018; 265: 2260–2266.

Cordani C, Meani A, Esposito F, Valsasina P, Colombo B, Pagani E, et al. Imaging correlates of hand motor performance in multiple sclerosis: A multiparametric structural and functional MRI study. Mult Scler 2019: 1352458518822145.

Dalton CM, Chard DT, Davies GR, Miszkiel KA, Altmann DR, Fernando K, et al. Early development of multiple sclerosis is associated with progressive grey matter atrophy in patients presenting with clinically isolated syndromes. Brain 2004; 127: 1101–1107.

De Stefano N, Airas L, Grigoriadis N, Mattle HP, O'Riordan J, Oreja-Guevara C, et al. Clinical relevance of brain volume measures in multiple sclerosis. CNS Drugs 2014; 28: 147–156.

Diedenhofen B, Musch J. cocor: A Comprehensive Solution for the Statistical Comparison of Correlations. PLOS ONE 2015; 10: e0121945.

Dogonowski A-M, Siebner HR, Sørensen PS, Wu X, Biswal B, Paulson OB, et al. Expanded functional coupling of subcortical nuclei with the motor resting-state network in multiple sclerosis. Mult Scler 2013; 19: 559–566.

Douaud G, Groves AR, Tamnes CK, Westlye LT, Duff EP, Engvig A, et al. A common brain network links development, aging, and vulnerability to disease. PNAS 2014; 111: 17648–17653.

Eden D, Gros C, Badji A, Dupont SM, De Leener B, Maranzano J, et al. Spatial distribution of multiple sclerosis lesions in the cervical spinal cord. Brain 2019

Eijlers AJC, van Geest Q, Dekker I, Steenwijk MD, Meijer KA, Hulst HE, et al. Predicting cognitive decline in multiple sclerosis: A 5-year follow-up study. Brain 2018; 141: 2605–2618.

Enzinger C, Barkhof F, Ciccarelli O, Filippi M, Kappos L, Rocca MA, et al. Nonconventional MRI and microstructural cerebral changes in multiple sclerosis. Nat Rev Neurol 2015; 11: 676–686.

Enzinger C, Pinter D, Rocca MA, De Luca J, Sastre-Garriga J, Audoin B, et al. Longitudinal fMRI studies: Exploring brain plasticity and repair in MS. Mult Scler 2016; 22: 269–278.

Eshaghi A, Bodini B, Ridgway GR, García-Lorenzo D, Tozer DJ, Sahraian MA, et al. Temporal and spatial evolution of grey matter atrophy in primary progressive multiple sclerosis. NeuroImage 2014; 86: 257–264.

Eshaghi A, Prados F, Brownlee WJ, Altmann DR, Tur C, Cardoso MJ, et al. Deep gray matter volume loss drives disability worsening in multiple sclerosis. Ann Neurol 2018; 83: 210–222.

Filippi M, Bar-Or A, Piehl F, Preziosa P, Solari A, Vukusic S, et al. Multiple sclerosis. Nat Rev Dis Primers 2018; 4: 43.

Filippi M, Brück W, Chard D, Fazekas F, Geurts JJG, Enzinger C, et al. Association between pathological and MRI findings in multiple sclerosis. Lancet Neurol 2019; 18: 198–210.

Filippi M, Pagani E, Preziosa P, Rocca MA. The Role of DTI in Multiple Sclerosis and Other Demyelinating Conditions. In: Van Hecke W, Emsell L, Sunaert S, editor(s). Diffusion Tensor Imaging: A Practical Handbook. New York, NY: Springer New York; 2016. p. 331–341

Filippi M, Preziosa P, Banwell BL, Barkhof F, Ciccarelli O, De Stefano N, et al. Assessment of lesions on magnetic resonance imaging in multiple sclerosis: Practical guidelines. Brain 2019

Filippi M, Preziosa P, Copetti M, Riccitelli G, Horsfield MA, Martinelli V, et al. Gray matter damage predicts the accumulation of disability 13 years later in MS. Neurology 2013; 81: 1759–1767.

Filippi M, Preziosa P, Rocca MA. Brain mapping in multiple sclerosis: Lessons learned about the human brain [Internet]. NeuroImage 2017[cited 2018 Jun 13] Available from: http://www.sciencedirect.com/science/article/pii/S1053811917307693

Filippi M, Preziosa P, Rocca MA. MRI in multiple sclerosis: What is changing? Curr Opin Neurol 2018; 31: 386–395.

Filippi M, Preziosa P, Rocca MA. Brain mapping in multiple sclerosis: Lessons learned about the human brain. Neuroimage 2019; 190: 32–45.

Filippi M, Rocca MA. MR imaging of gray matter involvement in multiple sclerosis: Implications for understanding disease pathophysiology and monitoring treatment efficacy. AJNR Am J Neuroradiol 2010; 31: 1171–1177.

Filippi M, Rocca MA, Barkhof F, Brück W, Chen JT, Comi G, et al. Association between pathological and MRI findings in multiple sclerosis. Lancet Neurol 2012; 11: 349–360.

Filippi M, Rocca MA, Ciccarelli O, De Stefano N, Evangelou N, Kappos L, et al. MRI criteria for the diagnosis of multiple sclerosis: MAGNIMS consensus guidelines. Lancet Neurol 2016; 15: 292–303.

Fisher E, Lee J-C, Nakamura K, Rudick RA. Gray matter atrophy in multiple sclerosis: A longitudinal study. Ann Neurol 2008; 64: 255–265.

Fortin J-P, Cullen N, Sheline YI, Taylor WD, Aselcioglu I, Cook PA, et al. Harmonization of cortical thickness measurements across scanners and sites. NeuroImage 2018; 167: 104–120.

Fortin J-P, Parker D, Tunç B, Watanabe T, Elliott MA, Ruparel K, et al. Harmonization of multi-site diffusion tensor imaging data. NeuroImage 2017; 161: 149–170.

Francx W, Llera A, Mennes M, Zwiers MP, Faraone SV, Oosterlaan J, et al. Integrated analysis of gray and white matter alterations in attention-deficit/hyperactivity disorder. NeuroImage: Clinical 2016; 11: 357–367.

Gallo A, Esposito F, Sacco R, Docimo R, Bisecco A, Della Corte M, et al. Visual resting-state network in relapsing-remitting MS with and without previous optic neuritis. Neurology 2012; 79: 1458–1465.

Geest Q van, Hulst HE, Meijer KA, Hoyng L, Geurts JJG, Douw L. The importance of hippocampal dynamic connectivity in explaining memory function in multiple sclerosis. Brain and Behavior 2018; 8: e00954.

Geurts JJG, Calabrese M, Fisher E, Rudick RA. Measurement and clinical effect of grey matter pathology in multiple sclerosis. Lancet Neurol 2012; 11: 1082–1092.

Giorgio A, De Stefano N. Advanced Structural and Functional Brain MRI in Multiple Sclerosis. Semin Neurol 2016; 36: 163–176.

Giorgio A, Palace J, Johansen-Berg H, Smith SM, Ropele S, Fuchs S, et al. Relationships of brain white matter microstructure with clinical and MR measures in relapsing-remitting multiple sclerosis. J Magn Reson Imaging 2010; 31: 309–316.

Giorgio A, Zhang J, Stromillo ML, Rossi F, Battaglini M, Nichelli L, et al. Pronounced Structural and Functional Damage in Early Adult Pediatric-Onset Multiple Sclerosis with No or Minimal Clinical Disability. Front Neurol 2017; 8: 608.

Groves AR, Beckmann CF, Smith SM, Woolrich MW. Linked independent component analysis for multimodal data fusion. NeuroImage 2011; 54: 2198–2217.

Groves AR, Smith SM, Fjell AM, Tamnes CK, Walhovd KB, Douaud G, et al. Benefits of multi-modal fusion analysis on a large-scale dataset: Life-span patterns of inter-subject variability in cortical morphometry and white matter microstructure. NeuroImage 2012; 63: 365–380.

Gupta CN, Calhoun VD, Rachakonda S, Chen J, Patel V, Liu J, et al. Patterns of Gray Matter Abnormalities in Schizophrenia Based on an International Mega-analysis. Schizophr Bull 2015; 41: 1133–1142.

Habes M, Erus G, Toledo JB, Bryan N, Janowitz D, Doshi J, et al. Regional tract-specific white matter hyperintensities are associated with patterns to aging-related brain atrophy via vascular risk factors, but also independently. Alzheimers Dement (Amst) 2018; 10: 278–284.

Haider L, Simeonidou C, Steinberger G, Hametner S, Grigoriadis N, Deretzi G, et al. Multiple sclerosis deep grey matter: The relation between demyelination, neurodegeneration, inflammation and iron. J Neurol Neurosurg Psychiatry 2014: jnnp-2014-307712.

Haider L, Zrzavy T, Hametner S, Höftberger R, Bagnato F, Grabner G, et al. The topograpy of demyelination and neurodegeneration in the multiple sclerosis brain. Brain 2016; 139: 807–815.

Han X, Tian H, Han Z, Zhang C, Liu Y, Gu J, et al. Correlation between white matter damage and gray matter lesions in multiple sclerosis patients. Neural Regen Res 2017; 12: 787–794.

Harrigan RL, Smith AK, Lyttle B, Box B, Landman BA, Bagnato F, et al. Quantitative characterization of optic nerve atrophy in patients with multiple sclerosis [Internet]. Mult Scler J Exp Transl Clin 2017; 3[cited 2019 Oct 14] Available from: https://www.ncbi.nlm.nih.gov/pmc/articles/PMC5600307/

Hawellek DJ, Hipp JF, Lewis CM, Corbetta M, Engel AK. Increased functional connectivity indicates the severity of cognitive impairment in multiple sclerosis. Proc Natl Acad Sci U S A 2011; 108: 19066–19071.

Henry RG, Shieh M, Amirbekian B, Chung S, Okuda DT, Pelletier D. Connecting white matter injury and thalamic atrophy in clinically isolated syndromes. Journal of the Neurological Sciences 2009; 282: 61–66.

van den Heuvel MP, Hulshoff Pol HE. Exploring the brain network: A review on resting-state fMRI functional connectivity. European Neuropsychopharmacology 2010; 20: 519–534.

Hochmeister S, Grundtner R, Bauer J, Engelhardt B, Lyck R, Gordon G, et al. Dysferlin is a new marker for leaky brain blood vessels in multiple sclerosis. J Neuropathol Exp Neurol 2006; 65: 855–865.

Hua K, Zhang J, Wakana S, Jiang H, Li X, Reich DS, et al. Tract probability maps in stereotaxic spaces: Analyses of white matter anatomy and tract-specific quantification. NeuroImage 2008; 39: 336–347.

Hulst HE, Steenwijk MD, Versteeg A, Pouwels PJW, Vrenken H, Uitdehaag BMJ, et al. Cognitive impairment in MS: Impact of white matter integrity, gray matter volume, and lesions. Neurology 2013; 80: 1025–1032.

Jehna M, Langkammer C, Khalil M, Fuchs S, Reishofer G, Fazekas F, et al. An Exploratory Study on the Spatial Relationship Between Regional Cortical Volume Changes and White Matter Integrity in Multiple Sclerosis. Brain Connectivity 2013; 3: 255–264.

Jenkinson M, Smith S. A global optimisation method for robust affine registration of brain images. Med Image Anal 2001; 5: 143–156.

Kawachi I, Lassmann H. Neurodegeneration in multiple sclerosis and neuromyelitis optica. J Neurol Neurosurg Psychiatry 2017; 88: 137–145.

Kilsdonk ID, Jonkman LE, Klaver R, van Veluw SJ, Zwanenburg JJM, Kuijer JPA, et al. Increased cortical grey matter lesion detection in multiple sclerosis with 7 T MRI: A post-mortem verification study. Brain 2016; 139: 1472–1481.

Kincses Z, Ropele S, Jenkinson M, Khalil M, Petrovic K, Loitfelder M, et al. Lesion probability mapping to explain clinical deficits and cognitive performance in multiple sclerosis. Multiple Sclerosis Journal 2011; 17: 681–689.

Kingwell E, Marriott JJ, Jetté N, Pringsheim T, Makhani N, Morrow SA, et al. Incidence and prevalence of multiple sclerosis in Europe: A systematic review. BMC Neurol 2013; 13: 1–13.

Kolasinski J, Stagg CJ, Chance SA, DeLuca GC, Esiri MM, Chang E-H, et al. A combined post-mortem magnetic resonance imaging and quantitative histological study of multiple sclerosis pathology. Brain 2012; 135: 2938–2951.

Koubiyr I, Besson P, Deloire M, Charre-Morin J, Saubusse A, Tourdias T, et al. Dynamic modular-level alterations of structural-functional coupling in clinically isolated syndrome. Brain 2019

Kurtzke JF. Rating neurologic impairment in multiple sclerosis: An expanded disability status scale (EDSS). Neurology 1983; 33: 1444–1452.

Lahat D, Adali T, Jutten C. Multimodal Data Fusion: An Overview of Methods, Challenges, and Prospects. Proceedings of the IEEE 2015; 103: 1449–1477.

Lassmann H. Multiple Sclerosis Pathology. Cold Spring Harb Perspect Med 2018; 8

Lassmann H, Brück W, Lucchinetti CF. The immunopathology of multiple sclerosis: An overview. Brain Pathol 2007; 17: 210–218.

Lassmann H, van Horssen J, Mahad D. Progressive multiple sclerosis: Pathology and pathogenesis. Nat Rev Neurol 2012; 8: 647–656.

Lee TW, Girolami M, Sejnowski TJ. Independent component analysis using an extended infomax algorithm for mixed subgaussian and supergaussian sources. Neural Comput 1999; 11: 417–441.

Li Y-O, Adali T, Calhoun VD. Estimating the number of independent components for functional magnetic resonance imaging data. Hum Brain Mapp 2007; 28: 1251–1266.

Liang S, Li Y, Zhang Z, Kong X, Wang Q, Deng W, et al. Classification of First-Episode Schizophrenia Using Multimodal Brain Features: A Combined Structural and Diffusion Imaging Study. Schizophr Bull 2019; 45: 591–599.

Lin F, Yu C, Jiang T, Li K, Chan P. Diffusion tensor tractography-based group mapping of the pyramidal tract in relapsing-remitting multiple sclerosis patients. AJNR Am J Neuroradiol 2007; 28: 278–282.

Lin X, Tench CR, Morgan PS, Niepel G, Constantinescu CS. 'Importance sampling' in MS: Use of diffusion tensor tractography to quantify pathology related to specific impairment. J Neurol Sci 2005; 237: 13–19.

Liu S, Wang H, Song M, Lv L, Cui Y, Liu Y, et al. Linked 4-Way Multimodal Brain Differences in Schizophrenia in a Large Chinese Han Population. Schizophr Bull 2019; 45: 436–449.

Llera A, Wolfers T, Mulders P, Beckmann CF. Inter-individual differences in human brain structure and morphometry link to variation in demographics and behavior. Elife 2019; 8

Llera A, Wolfers T, Mulders P, Beckmann CF. Inter-individual differences in human brain structure and morphology link to variation in demographics and behavior. eLife 2019; 8: e44443.

Loitfelder M, Filippi M, Rocca M, Valsasina P, Ropele S, Jehna M, et al. Abnormalities of Resting State Functional Connectivity Are Related to Sustained Attention Deficits in MS. PLOS ONE 2012; 7: e42862.

Louapre C, Perlbarg V, García-Lorenzo D, Urbanski M, Benali H, Assouad R, et al. Brain networks disconnection in early multiple sclerosis cognitive deficits: An anatomofunctional study. Human Brain Mapping 2014; 35: 4706–4717.

Lublin FD, Reingold SC, Cohen JA, Cutter GR, Sørensen PS, Thompson AJ, et al. Defining the clinical course of multiple sclerosis: The 2013 revisions. Neurology 2014; 83: 278–286.

Lucchinetti C, Brück W, Parisi J, Scheithauer B, Rodriguez M, Lassmann H. Heterogeneity of multiple sclerosis lesions: Implications for the pathogenesis of demyelination. Ann Neurol 2000; 47: 707–717.

Machado-Santos J, Saji E, Tröscher AR, Paunovic M, Liblau R, Gabriely G, et al. The compartmentalized inflammatory response in the multiple sclerosis brain is composed of tissue-resident CD8+ T lymphocytes and B cells. Brain 2018; 141: 2066–2082.

Mahad DH, Trapp BD, Lassmann H. Pathological mechanisms in progressive multiple sclerosis. Lancet Neurol 2015; 14: 183–193.

Manning KY, Llera A, Dekaban GA, Bartha R, Barreira C, Brown A, et al. Linked MRI signatures of the brain's acute and persistent response to concussion in female varsity rugby players. Neuroimage Clin 2019; 21: 101627.

Maudoux A, Lefebvre P, Cabay J-E, Demertzi A, Vanhaudenhuyse A, Laureys S, et al. Auditory Resting-State Network Connectivity in Tinnitus: A Functional MRI Study. PLOS ONE 2012; 7: e36222.

McDonald WI, Compston A, Edan G, Goodkin D, Hartung HP, Lublin FD, et al. Recommended diagnostic criteria for multiple sclerosis: Guidelines from the International Panel on the diagnosis of multiple sclerosis. Ann Neurol 2001; 50: 121–127.

Meijer KA, Cercignani M, Muhlert N, Sethi V, Chard D, Geurts JJG, et al. Patterns of white matter damage are non-random and associated with cognitive function in secondary progressive multiple sclerosis. NeuroImage: Clinical 2016; 12: 123–131.

Meijer KA, van Geest Q, Eijlers AJC, Geurts JJG, Schoonheim MM, Hulst HE. Is impaired information processing speed a matter of structural or functional damage in MS? NeuroImage: Clinical 2018; 20: 844–850.

Mesaros S, Rocca MA, Kacar K, Kostic J, Copetti M, Stosic-Opincal T, et al. Diffusion tensor MRI tractography and cognitive impairment in multiple sclerosis. Neurology 2012; 78: 969–975.

Mesaros S, Rovaris M, Pagani E, Pulizzi A, Caputo D, Ghezzi A, et al. A Magnetic Resonance Imaging Voxel-Based Morphometry Study of Regional Gray Matter Atrophy in Patients With Benign Multiple Sclerosis. Arch Neurol 2008; 65: 1223–1230.

Moll NM, Rietsch AM, Thomas S, Ransohoff AJ, Lee J-C, Fox R, et al. Multiple Sclerosis Normal-Appearing White Matter: Pathology-Imaging Correlations. Ann Neurol 2011; 70: 764–773.

Mollink J, Smith SM, Elliott LT, Kleinnijenhuis M, Hiemstra M, Alfaro-Almagro F, et al. The spatial correspondence and genetic influence of interhemispheric connectivity with white matter microstructure. Nature Neuroscience 2019: 1.

Narayana PA, Govindarajan KA, Goel P, Datta S, Lincoln JA, Cofield SS, et al. Regional cortical thickness in relapsing remitting multiple sclerosis: A multi-center study. Neuroimage Clin 2012; 2: 120–131.

Nickerson LD, Smith SM, Öngür D, Beckmann CF. Using Dual Regression to Investigate Network Shape and Amplitude in Functional Connectivity Analyses. Front Neurosci 2017; 11: 115.

Oishi K, Faria A, Jiang H, Li X, Akhter K, Zhang J, et al. Atlas-based whole brain white matter analysis using large deformation diffeomorphic metric mapping: Application to normal elderly and Alzheimer's disease participants. Neuroimage 2009; 46: 486–499.

Olsson T, Barcellos LF, Alfredsson L. Interactions between genetic, lifestyle and environmental risk factors for multiple sclerosis. Nat Rev Neurol 2017; 13: 25–36.

Pagani E, Filippi M, Rocca MA, Horsfield MA. A method for obtaining tract-specific diffusion tensor MRI measurements in the presence of disease: Application to patients with clinically isolated syndromes suggestive of multiple sclerosis. Neuroimage 2005; 26: 258–265.

Parmar K, Stadelmann C, Rocca MA, Langdon D, D'Angelo E, D'Souza M, et al. The role of the cerebellum in multiple sclerosis—150 years after Charcot. Neuroscience & Biobehavioral Reviews 2018; 89: 85–98.

Polman CH, Reingold SC, Banwell B, Clanet M, Cohen JA, Filippi M, et al. Diagnostic criteria for multiple sclerosis: 2010 Revisions to the McDonald criteria. Ann Neurol 2011; 69: 292–302.

Popescu V, Klaver R, Voorn P, Galis-de Graaf Y, Knol DL, Twisk JWR, et al. What drives MRI-measured cortical atrophy in multiple sclerosis? Mult Scler 2015; 21: 1280–1290.

Prinster A, Quarantelli M, Lanzillo R, Orefice G, Vacca G, Carotenuto B, et al. A voxel-based morphometry study of disease severity correlates in relapsing–remitting multiple sclerosis. Mult Scler 2010; 16: 45–54.

Pruim RHR, Mennes M, van Rooij D, Llera A, Buitelaar JK, Beckmann CF. ICA-AROMA: A robust ICA-based strategy for removing motion artifacts from fMRI data. Neuroimage 2015; 112: 267–277.

Rao SM. A manual for the brief repeatable battery of neuropsychological tests in multiple sclerosis. Milwaukee: Medical College of Wisconsin 1990

Rawji KS, Mishra MK, Yong VW. Regenerative Capacity of Macrophages for Remyelination. Front Cell Dev Biol 2016; 4: 47.

Reich DS, Lucchinetti CF, Calabresi PA. Multiple Sclerosis. New England Journal of Medicine 2018; 378: 169–180.

Riccitelli G, Rocca MA, Pagani E, Rodegher ME, Rossi P, Falini A, et al. Cognitive impairment in multiple sclerosis is associated to different patterns of gray matter atrophy according to clinical phenotype. Human Brain Mapping 2011; 32: 1535–1543.

Rocca MA, Amato MP, De Stefano N, Enzinger C, Geurts JJ, Penner I-K, et al. Clinical and imaging assessment of cognitive dysfunction in multiple sclerosis. Lancet Neurol 2015; 14: 302–317.

Rocca MA, Battaglini M, Benedict RHB, De Stefano N, Geurts JJG, Henry RG, et al. Brain MRI atrophy quantification in MS: From methods to clinical application. Neurology 2017; 88: 403–413.

Rocca MA, Horsfield MA, Sala S, Copetti M, Valsasina P, Mesaros S, et al. A multicenter assessment of cervical cord atrophy among MS clinical phenotypes. Neurology 2011; 76: 2096–2102.

Rocca MA, Valsasina P, Absinta M, Riccitelli G, Rodegher ME, Misci P, et al. Default-mode network dysfunction and cognitive impairment in progressive MS. Neurology 2010; 74: 1252–1259.

Rocca MA, Valsasina P, Leavitt VM, Rodegher M, Radaelli M, Riccitelli GC, et al. Functional network connectivity abnormalities in multiple sclerosis: Correlations with disability and cognitive impairment. Mult Scler 2018; 24: 459–471.

Rocca MA, Valsasina P, Martinelli V, Misci P, Falini A, Comi G, et al. Large-scale neuronal network dysfunction in relapsing-remitting multiple sclerosis. Neurology 2012: WNL.0b013e31826d5f10.

Roosendaal SD, Bendfeldt K, Vrenken H, Polman CH, Borgwardt S, Radue EW, et al. Grey matter volume in a large cohort of MS patients: Relation to MRI parameters and disability. Mult Scler 2011; 17: 1098–1106.

Roosendaal SD, Geurts JJG, Vrenken H, Hulst HE, Cover KS, Castelijns JA, et al. Regional DTI differences in multiple sclerosis patients. NeuroImage 2009; 44: 1397–1403.

Rossi F, Giorgio A, Battaglini M, Stromillo ML, Portaccio E, Goretti B, et al. Relevance of Brain Lesion Location to Cognition in Relapsing Multiple Sclerosis [Internet]. PLoS One 2012; 7Available from: http://www.ncbi.nlm.nih.gov/pmc/articles/PMC3489883/

Ruckh JM, Zhao J-W, Shadrach JL, van Wijngaarden P, Rao TN, Wagers AJ, et al. Rejuvenation of regeneration in the aging central nervous system. Cell Stem Cell 2012; 10: 96–103.

Sailer M, Fischl B, Salat D, Tempelmann C, Schönfeld MA, Busa E, et al. Focal thinning of the cerebral cortex in multiple sclerosis. Brain 2003; 126: 1734–1744.

Scalfari A, Romualdi C, Nicholas RS, Mattoscio M, Magliozzi R, Morra A, et al. The cortical damage, early relapses, and onset of the progressive phase in multiple sclerosis. Neurology 2018; 90: e2107–e2118.

Schoonheim MM, Hulst HE, Brandt RB, Strik M, Wink AM, Uitdehaag BMJ, et al. Thalamus structure and function determine severity of cognitive impairment in multiple sclerosis. Neurology 2015; 84: 776–783.

Sepulcre J, Masdeu JC, Pastor MA, Goñi J, Barbosa C, Bejarano B, et al. Brain pathways of verbal working memory: A lesion-function correlation study. Neuroimage 2009; 47: 773–778.

Sethi V, Yousry TA, Muhlert N, Ron M, Golay X, Wheeler-Kingshott C, et al. Improved detection of cortical MS lesions with phase-sensitive inversion recovery MRI. J Neurol Neurosurg Psychiatry 2012; 83: 877–882.

Simpson S, Blizzard L, Otahal P, Van der Mei I, Taylor B. Latitude is significantly associated with the prevalence of multiple sclerosis: A meta-analysis. J Neurol Neurosurg Psychiatry 2011; 82: 1132–1141.

Smith S, Duff E, Groves A, Nichols TE, Jbabdi S, Westlye LT, et al. Structural variability in the human brain reflects fine-grained functional architecture at the population level. J Neurosci 2019: 2912–18.

Smith SM. The future of FMRI connectivity. NeuroImage 2012; 62: 1257–1266.

Smith SM, Fox PT, Miller KL, Glahn DC, Fox PM, Mackay CE, et al. Correspondence of the brain's functional architecture during activation and rest. PNAS 2009; 106: 13040–13045.

Smith SM, Jenkinson M, Johansen-Berg H, Rueckert D, Nichols TE, Mackay CE, et al. Tract-based spatial statistics: Voxelwise analysis of multi-subject diffusion data. Neuroimage 2006; 31: 1487–1505.

Solaro C, Brichetto G, Amato MP, Cocco E, Colombo B, D'Aleo G, et al. The prevalence of pain in multiple sclerosis: A multicenter cross-sectional study. Neurology 2004; 63: 919–921.

Steenwijk MD, Daams M, Pouwels PJW, Balk LJ, Tewarie PK, Killestein J, et al. What Explains Gray Matter Atrophy in Long-standing Multiple Sclerosis? Radiology 2014; 272: 832–842.

Steenwijk MD, Geurts JJG, Daams M, Tijms BM, Wink AM, Balk LJ, et al. Cortical atrophy patterns in multiple sclerosis are non-random and clinically relevant. Brain 2016; 139: 115–126.

Stefano ND, Stromillo ML, Giorgio A, Bartolozzi ML, Battaglini M, Baldini M, et al. Establishing pathological cut-offs of brain atrophy rates in multiple sclerosis. J Neurol Neurosurg Psychiatry 2016; 87: 93–99.

Sui J, Qi S, Erp TGM van, Bustillo J, Jiang R, Lin D, et al. Multimodal neuromarkers in schizophrenia via cognition-guided MRI fusion. Nature Communications 2018; 9: 3028.

Sumowski JF, Benedict R, Enzinger C, Filippi M, Geurts JJ, Hamalainen P, et al. Cognition in multiple sclerosis: State of the field and priorities for the future. Neurology 2018; 90: 278–288.

Sumowski JF, Rocca MA, Leavitt VM, Dackovic J, Mesaros S, Drulovic J, et al. Brain reserve and cognitive reserve protect against cognitive decline over 4.5 years in MS. Neurology 2014; 82: 1776–1783.

Tahedl M, Levine SM, Greenlee MW, Weissert R, Schwarzbach JV. Functional Connectivity in Multiple Sclerosis: Recent Findings and Future Directions [Internet]. Front Neurol 2018; 9[cited 2019 Jul 29] Available from: https://www.ncbi.nlm.nih.gov/pmc/articles/PMC6193088/

Tewarie P, Steenwijk MD, Brookes MJ, Uitdehaag BMJ, Geurts JJG, Stam CJ, et al. Explaining the heterogeneity of functional connectivity findings in multiple sclerosis: An empirically informed modeling study. Hum Brain Mapp 2018; 39: 2541–2548.

Thompson AJ, Banwell BL, Barkhof F, Carroll WM, Coetzee T, Comi G, et al. Diagnosis of multiple sclerosis: 2017 revisions of the McDonald criteria. Lancet Neurol 2018; 17: 162–173.

Vellinga MM, Geurts JJG, Rostrup E, Uitdehaag BMJ, Polman CH, Barkhof F, et al. Clinical correlations of brain lesion distribution in multiple sclerosis. Journal of Magnetic Resonance Imaging 2009; 29: 768–773.

Wallin MT, Culpepper WJ, Nichols E, Bhutta ZA, Gebrehiwot TT, Hay SI, et al. Global, regional, and national burden of multiple sclerosis 1990–2016: A systematic analysis for the Global Burden of Disease Study 2016. The Lancet Neurology 2019; 18: 269–285.

Welton T, Kent D, Constantinescu CS, Auer DP, Dineen RA. Functionally Relevant White Matter Degradation in Multiple Sclerosis: A Tract-based Spatial Meta-Analysis. Radiology 2014; 275: 89–96.

Wilson M, Tench C, Morgan P, Blumhardt L. Pyramidal tract mapping by diffusion tensor magnetic resonance imaging in multiple sclerosis: Improving correlations with disability. J Neurol Neurosurg Psychiatry 2003; 74: 203–207.

Winkler AM, Webster MA, Brooks JC, Tracey I, Smith SM, Nichols TE. Non-parametric combination and related permutation tests for neuroimaging. Hum Brain Mapp 2016; 37: 1486–1511.

Wolfers T, Arenas AL, Onnink AMH, Dammers J, Hoogman M, Zwiers MP, et al. Refinement by integration: Aggregated effects of multimodal imaging markers on adult ADHD. J Psychiatry Neurosci 2017; 42: 160240.

Wu Z-M, Llera A, Hoogman M, Cao Q-J, Zwiers MP, Bralten J, et al. Linked anatomical and functional brain alterations in children with attention-deficit/hyperactivity disorder. NeuroImage: Clinical 2019; 23: 101851.

Xu L, Groth KM, Pearlson G, Schretlen DJ, Calhoun VD. Source-Based Morphometry: The Use of Independent Component Analysis to Identify Gray Matter Differences With Application to Schizophrenia. Hum Brain Mapp 2009; 30: 711–724.

Yamashita M, Yoshihara Y, Hashimoto R, Yahata N, Ichikawa N, Sakai Y, et al. A prediction model of working memory across health and psychiatric disease using whole-brain functional connectivity. eLife 2018; 7: e38844.

Yeo BTT, Krienen FM, Sepulcre J, Sabuncu MR, Lashkari D, Hollinshead M, et al. The organization of the human cerebral cortex estimated by intrinsic functional connectivity. Journal of Neurophysiology 2011; 106: 1125–1165.

Yu HJ, Christodoulou C, Bhise V, Greenblatt D, Patel Y, Serafin D, et al. Multiple white matter tract abnormalities underlie cognitive impairment in RRMS. NeuroImage 2012; 59: 3713–3722.

Yu M, Linn KA, Cook PA, Phillips ML, McInnis M, Fava M, et al. Statistical harmonization corrects site effects in functional connectivity measurements from multi-site fMRI data. Hum Brain Mapp 2018; 39: 4213–4227.

Yu M, Linn KA, Shinohara RT, Oathes DJ, Cook PA, Duprat R, et al. Childhood trauma history is linked to abnormal brain connectivity in major depression. PNAS 2019; 116: 8582–8590.

Zeis T, Graumann U, Reynolds R, Schaeren-Wiemers N. Normal-appearing white matter in multiple sclerosis is in a subtle balance between inflammation and neuroprotection. Brain 2008; 131: 288–303.

Zipoli V, Goretti B, Hakiki B, Siracusa G, Sorbi S, Portaccio E, et al. Cognitive impairment predicts conversion to multiple sclerosis in clinically isolated syndromes. Mult Scler 2010; 16: 62–67.

Zurawski J, Lassmann H, Bakshi R. Use of Magnetic Resonance Imaging to Visualize Leptomeningeal Inflammation in Patients With Multiple Sclerosis: A Review. JAMA Neurol 2017; 74: 100–109.

9 Acknowledgments

First, my thanks go to Professor Nicola De Stefano for guiding me through the maze of the PhD at Quantitative Neuroimaging Lab (QNL). Thank you for opening the door without rejection, when I stood outside knocking on the door of neuroimaging. His guidance was invaluable for helping me arrive here today.

My deepest gratitude goes to Dr. Antonio Giorgio for being my mentor in the field of neuroimaging and friend since the beginning of my experience in Siena. I would especially like to acknowledge and thank you for believing in me as well as for the possibility of keeping an active and fruitful scientific collaboration over these years.

My warmest thanks go to Marco Battaglini. Thank you for not only being a friend but someone with whom I have the immense pleasure of exchanging ideas and getting support on segmentation and registration. The overnight train to MAGNIMS meeting was a special experience for us.

Very special thanks go to Riccardo Tappa Brocci for always giving me a hand. Thank you for guiding me in the field of lesion and atrophy.

Thanks to Dr. Claudia Vinciguerra for not only being a close friend but someone with whom I have shared the thinking of research and I've always been supported for the cognition implications. I have enjoyed the many coffees and lively discussions that we have had over these years.

I would like to thank Ludovico Luchetti and Giordano Gentile for their support in our collaborative efforts.

I would like to thank Dr. Maria Laura Stromillo for her constant help and support.

The support from my colleagues at the QNL and Toscana Life Sciences (TLS), especially Irina Efimenko and Giacomo Demurtas, needs to be acknowledged.

I would like to thank Loriana Bocci and Xiaoke Zhong. Without your help, I could not come back to Siena for neuroimaging. Both of you have been incredibly supportive in my life in Siena since the very beginning.

Of course, thanks must go to my parents. My parents tried their best to support me to do what I want. Without their constant support, I would never have had a chance to start and finish a PhD.

Finally, none of this work would have been possible without the unconditional love from my wife Yashan and son Xun. Their unwavering support and encouragement allowed me to focus on my work at times when it seemed neverending. There is so much I want to say but so little that can be expressed. I would like to thank my wife and son for everything they did for me.